J. Phys.: Condens. Matter **11** (1999) 9303–9346. Printed in the UK PII: S0953-8984(99)07194-5

REVIEW ARTICLE

Magnetism of chromium at surfaces, at interfaces and in thin films

Hartmut Zabel

Fakultät für Physik und Astronomie, Institut für Experimentalphysik/Festkörperphysik, Ruhr-Universität Bochum, D 44780 Bochum, Germany

Received 25 August 1999

Abstract. The spin density wave (SDW) magnetism of thin epitaxial Cr films has recently become the focus of interest because of its mediating role in exchange coupled superlattices. While the incommensurate SDW magnetism and the Néel temperature are well established for bulk Cr, the question arises of how these properties are altered in thin films and superlattices either due to dimensionality effects or due to proximity with the ferromagnetic or paramagnetic boundary layers. After a brief introduction to the basic properties of bulk Cr, this review provides an overview of the SDW magnetism in thin Cr films, starting with surface properties and continuing with the discussion of Cr films of various thickness. The emphasis is more on SDW order in different confined environments than on exchange coupling. The scaling of the Néel temperature with thickness, the critical thickness for the onset of SDW order, the orientation of the SDW wave vector in different environments and the enhancement of SDW order due to proximity effects are extensively discussed. Most important is the role of the interface roughness in case of contact with a ferromagnetic layer. Conflicting results obtained with different experimental techniques are critically reviewed and an interpretation of the SDW order depending on interface quality is proposed.

1. Introduction

The incommensurate spin density wave (SDW) magnetism of Cr has fascinated many researchers since its first discovery via neutron scattering in 1959 by two independent groups in Brookhaven [1] and in Leningrad [2]. Although the satellite peaks were first interpreted in terms of antiphase domain boundaries, their explanation as a manifestation of an incommensurate spin density wave followed soon after by Overhauser [3]. In thin films the magnetism of Cr has recently become the focus of interest because of its mediating role in exchange coupled superlattices and GMR materials [4]. While the magnetic phase diagram and the Néel temperature, $T_N = 311$ K, are well established properties for bulk Cr, the question arises of how they are altered in thin films and superlattices either due to dimensionality effects or due to the proximity with ferromagnetic or paramagnetic boundary layers. The early scattering experiments were performed on large single crystals. Unravelling the spin density wave magnetism in thin films is not an easy task. Usual experimental techniques for studying magnetism are not applicable because of the antiferromagnetic nature of Cr. The most direct techniques, neutron and x-ray scattering, are difficult to apply because of the small scattering volume. Nevertheless, these methods remain the most suitable ones even for thin film investigations. In addition a number of indirect methods have been utilized to unravel the magnetic state in thin Cr films. Those are either nuclear probe techniques, domain imaging of ferromagnetic layers on top of Cr or magnetic hysteresis measurements of ferromagnet/Cr

0953-8984/99/489303+44$30.00

heterostructures. Thin films of Cr are also of interest because of predictions concerning their surface magnetic properties. It has been proposed that Cr possesses an enhanced magnetic moment exceeding the bulk value by a factor of 3–4 and that (001) oriented layers are ordered in alternating ferromagnetic monolayers with opposite magnetization direction. The possibility of unveiling the intriguing magnetic properties of Cr films and surfaces relies on the capabilities of growing well ordered epitaxial films. Assuming perfect layers, interfaces and surfaces, a number of issues are of interest such as:

(1) the mechanism for the formation of a spin density wave in thin films as compared to the bulk;
(2) the critical thickness for Cr to develop an SDW order;
(3) the scaling of the Néel temperature with the Cr film thickness;
(4) the magnetic moment in thin Cr films in the commensurate and incommensurate SDW state, and at surfaces;
(5) the boundary conditions for the SDW to be fulfilled at interfaces between Cr and ferromagnetic or paramagnetic materials and the position of the nodes with respect to the interface;
(6) the enhancement or suppression of SDW order due to proximity effects;
(7) the magnetic domain structure of Cr in confined environments;
(8) the dependence of the polarization, wave vector and amplitude of the SDW on proximity effects, growth properties, epitaxial strain and epitaxial relationships;
(9) the effect of interface roughness on the polarization and orientation of the SDW in Cr films.

Considerable theoretical and experimental effort has been devoted in recent years to the understanding of SDW order in Cr subjected to confined environments with specific boundary conditions. This review attempts to describe the current status of the field and examines open questions remaining for future work. The exchange coupling in magnetic heterostructures mediated by the Cr spacer will not be discussed here. This will be the subject of other contributions in this volume provided by Parkin and Bruno. On the other hand, exchange coupling often serves as an important tool for obtaining information on the magnetic state of Cr in thin films. The main emphasis will, however, be on the magnetic state and structure of thin Cr films. It is clear that such a short review cannot be comprehensive. Therefore only some main results will be discussed without attempting completeness. We will start with a short overview of the bulk properties of Cr, continue with an overview of theoretical predictions for the bulk, surface and thin film cases in section 3, introduce the most frequently applied experimental techniques in section 4 and finally review experimental investigations of structural and magnetic properties of Cr surfaces and thin films in section 5. We close with a discussion and summary of the current status of the field in section 6.

2. Bulk properties

An excellent and extensive review of the bulk properties of Cr was given by Fawcett about 10 years ago [5], and the reader is referred to this work for any details. Chromium has a bcc structure with a lattice parameter of $a_{Cr} = 2.884$ Å in the paramagnetic state. As a 3d metal Cr has to be considered an itinerant antiferromagnet. If Cr had a commensurate antiferromagnetic structure, the magnetic moment density at the corners would be opposite to the ones at the

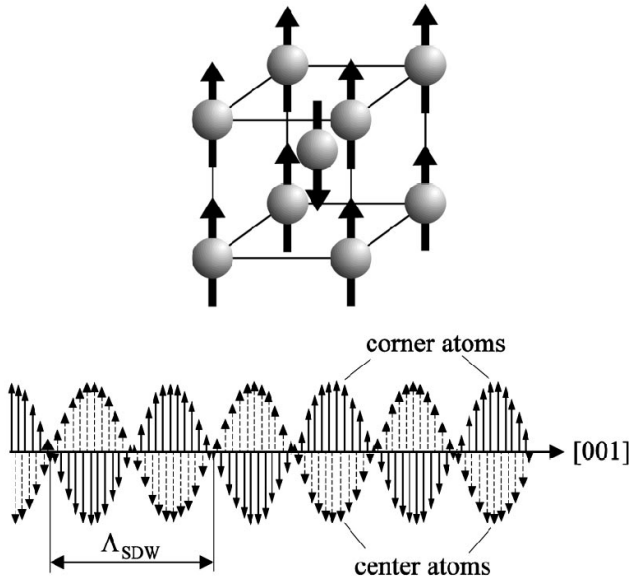

Figure 1. Commensurate and incommensurate spin density wave structure of bcc Cr. In the lower panel a transverse SDW is sketched with wave vector in the [001] direction and magnetic moments normal to the wave vector.

centre of the bcc unit cell, as sketched in figure 1(a), forming a commensurate spin density wave (C-SDW) structure with a wave vector of

$$\vec{Q}_{com} = \frac{2\pi}{a_{Cr}}[001] = \frac{2\pi}{\Lambda}[001] = \vec{G}_{\{001\}} = \{0, 0, 1\} \tag{1}$$

where $\Lambda = a_{Cr}$ is the periodicity of the C-SDW. Thus the antiferromagnetic bcc structure consists of a sequence of ferromagnetic (001) planes with alternating spin direction. Furthermore, the magnetic moments can be oriented parallel to any of the $\{0, 0, 1\}$ crystallographic axes. Therefore, in thermal equilibrium three different domains are expected to co-exist for the different orientations of the magnetic moments. Pure Cr exhibits, in fact, a linearly polarized incommensurate spin density wave (I-SDW) structure, which consists of a sinusoidal modulation of the magnetic moments:

$$\vec{\mu}(\vec{r}) = \vec{\mu}_0 \sin(\vec{Q}_{\pm}\vec{r}) \tag{2}$$

with an amplitude μ_0 of about 0.5 μ_B/atom at 4.2 K [6] and an incommensurate wave vector $\vec{Q}_{\pm}$ given by

$$\vec{Q}_{\pm} = \left(\frac{2\pi}{a_{Cr}} - \frac{2\pi}{\Lambda_{SDW}}\right)[001] = \frac{2\pi}{a_{Cr}}(1-\delta) = \vec{G}_{\{001\}}(1-\delta) = \{0, 0, 1-\delta\} \tag{3}$$

where δ is a measure of the deviation from the commensurability and Λ_{SDW} is the periodicity of the incommensurate SDW. The I-SDW is schematically shown in figure 1(*b*) and can be visualized as a spin lattice which is slightly expanded as compared to the crystal lattice, yielding a beating effect between both with a beat periodicity of $\Lambda_{SDW} = a/\delta$ and a number $1/\delta$ of Cr monolayers (ML) between any successive nodes. Since δ is about 5%, Λ_{SDW} amounts to about 60 Å. Λ_{SDW} increases smoothly from 60 Å at 10 K to 78 Å at the Néel temperature $T_N = 311$ K, corresponding to an increase from 42 to 54 Cr ML for a full period or 21 to

27 ML between the nodes in the [001] direction, respectively. For a commensurate structure δ is zero.

Unlike the commensurate case, for an incommensurate SDW we need to distinguish between the orientation of the ordering wave vector $\vec{Q}_\pm$ and the polarization of the spins. $\vec{Q}_\pm$ can be oriented along any one of the three crystallographic {100} directions. The polarization may, however, be either longitudinal ($\vec{Q}_\pm \parallel \vec{\mu}$) or transverse ($\vec{Q}_\pm \perp \vec{\mu}$). At low temperatures the I-SDW has longitudinal character, referred to as the AF_2 phase. Usually all three orientations occur with equal probability in three different domains. At 123 K a first order spin flip transition occurs to a transverse I-SDW (AF_1 phase), now co-existing in six possible domains. The transverse I-SDW exhibits a weak first order Néel transition at 311 K [6, 7]. Above 311 K, Cr is a paramagnet. The bulk phase diagram is schematically reproduced in figure 2.

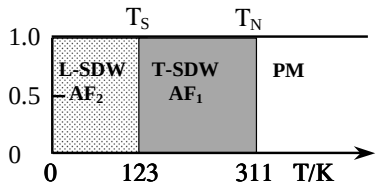

Figure 2. Schematic phase diagram of Cr. The vertical axis indicates the volume fraction of the respective phase. L-SDW or AF_2 and T-SDW or AF_1 refer to the longitudinal and transverse spin density wave in Cr below the Néel temperature at 311 K, PM designates the paramagnetic phase. At 123 K a first order spin flop transition from a longitudinal to a transverse spin density wave takes place.

In addition to the SDW, Cr exhibits a charge density wave (CDW) and a strain wave (SW) with half the period of the SDW. The SW can be considered as a periodic, longitudinal lattice modulation, similar to a frozen phonon. The origin of the SW has long been disputed. It may either be considered as arising from an exchange striction effect of the SDW [8], or as independently induced by an instability of Cr with respect to a CDW [9–11]. In the first model the wave vectors are related as $\vec{Q}_\pm^{SW} = 2\vec{Q}_\pm^{SDW}$, whereas in the second model the SW wave vector is not required to be strictly twice that for the SDW. Comparison of neutron scattering results determining $\vec{Q}_\pm^{SDW}$ by Werner *et al* [11] with x-ray scattering measurements of $\vec{Q}_\pm^{SW}$ by Gibbs *et al* [12] and Hill *et al* [13] show that they are indeed related by a factor of 2. Therefore in the bulk there is no reason to believe that the SDW and CDW/SW are two independent entities.

The close relationship between SDW and SW is also expressed by the crystal symmetry. In the paramagnetic phase Cr is cubic. In the AF_1 phase Cr has an orthorhombic crystal structure with the longest axis at T_N becoming the shortest at T_{SF}. In the AF_2 phase Cr is tetragonal. Thus the first order transition at T_{SF} is not only characterized by an L to T spin flip transition but also by a change of crystal symmetry from tetragonal to orthorhombic.

Under normal conditions bulk Cr forms a poly-domain state for $T < T_N$, i.e. domains exist with different orientations for $\vec{Q}_\pm$ and $\vec{\mu}$. A single domain state can, however, be achieved by cooling the sample through the Néel temperature either in a high external magnetic field or under uniaxial stress along one of the cube edges. Magnetic field cooling through T_N favours domains with $\vec{Q}_\pm$ parallel to $\vec{H}$ (Bastow and Street [14], Werner *et al* [11]). For instance, if $\vec{H}$ is parallel to [001] below T_N and then reduced to zero, $\vec{\mu}$ will be perpendicular to $\vec{H}$ and $\vec{Q}_\pm$ (spin flop phase) in the AF_1 phase (oriented either along [100] or [010]), and parallel to [001] in the AF_2 phase. Cooling through T_N with uniaxial tensile stress along [001] will also align $\vec{Q}_\pm$ parallel to the expanded axis [14]. This observation is important for the discussion of epitaxial and pseudomorphic Cr films with different residual strains depending on the substrate.

The SDW structure of Cr is usually incommensurate. Internal elastic strains or small grain sizes may cause the SDW to become commensurate. The commensurate antiferromagnetic structure is designated as the AF_0 phase. The AF_0 phase has a much higher Néel temperature

of about 475 K and a higher magnetic moment. Alloying has also a dramatic effect on the SDW state of Cr. For instance, doping with Mn increases the electron concentration (donor), whereas V decreases the electron concentration (acceptor). At the same time $\vec{Q}_{\pm}$, $|\vec{\mu}|$ and T_N increase (decrease) with Mn (V) doping. With only 0.3% Mn in Cr will result in a C-SDW with $\vec{Q}_{\pm} = 1$, $|\vec{\mu}| \cong 0.8\ \mu_B$ and $T_N = 600$ K [15, 16]. Vice versa, doping Cr with 2% V reduces the T_N to 50% of the bulk value and the node to node distance decreases from 21 to 13 ML at low temperatures [16].

3. Theory of SDW magnetism in CR

3.1. Bulk

Overhauser was first to point out that the paramagnetic state of an electron gas is unstable against the formation of a static spin density wave [3]. The instability occurs for a wave vector $\vec{Q} = 2k_F$, the diameter of the Fermi surface. In order to increase the contact area and therefore the interaction between spin up and spin down Fermi surfaces, $\vec{Q}$ should be slightly less than $2k_F$. For a spherical or slightly truncated Fermi surface this instability is rather weak. However, Lomer has shown that the Fermi surface of Cr exhibits a pronounced nesting property [17]. The electron and hole Fermi surfaces situated at the Γ and H points of the bcc reciprocal lattice, respectively, have nearly octahedral shape. This Fermi surface was later confirmed by a number of band structure calculations [18, 19], including a most recent *ab initio* calculation by Hirai [20]. Figure 3 shows the Fermi surface from the calculations of Laurent *et al* [18]. Because of the same shapes the electron 'jacks' and hole 'necks' effectively nest each other to induce a SDW instability. This implies that $\vec{Q}$, which measures the distance between the electron and hole octahedra, couples Bloch states of the electron band to Bloch states of the hole band such that the occupied states are lowered and the unoccupied states are lifted in energy. This effectively lowers the density of states at the Fermi level and stabilizes the SDW in Cr. Because the hole Fermi surface is slightly larger than the electron Fermi surface, the $\vec{Q}$

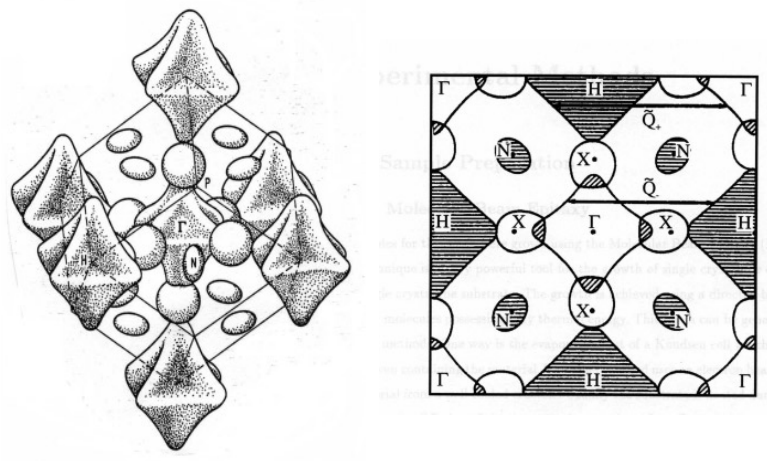

Figure 3. Fermi surface of Cr according to the band structure calculations of Laurent *et al* [18]: (a) three dimensional sketch of the Fermi surface; (b) projection into the (100) plane. The electron Fermi surface is centred at the origin of the Brillouin zone at Γ, while the hole Fermi surface is concentrated around the H-points in the reciprocal lattice. Q_- and Q_+ designate the nesting vectors between electron and hole states at the respective Fermi surface.

for the SDW is incommensurate. Thus the difference between the paramagnetic and the SDW phase is characterized by a saddle point at the incommensurate position $\vec{Q}$ in reciprocal space with an energy gap E_g of about 120 meV at $T = 0$. The opening of band gaps at the specified points in the reciprocal lattice becomes quite obvious in band structure calculations by Kübler [19], which compare the paramagnetic and antiferromagnetic state.

With increasing temperature the upper energy branch will be occupied at the expense of the lower energy branch. Since the upper branch has a spin polarization opposite to that of the lower branch, the overall result will be a reduction of the SDW amplitude with increasing temperature. At the same time the exchange potential will also be reduced, providing less polarization of each state and causing a further reduction of the SDW amplitude. Overhauser has pointed out the similarity between the theories of SDW and BCS superconductivity [3]. On the basis of this similarity the energy gap is predicted to vary with T/T_c in a similar fashion as in superconductors:

$$\frac{E_g(T)}{E_g(0)} = \sqrt{1 - \left(\frac{T}{T_N}\right)^{\beta}} \tag{4}$$

with an exponent β, depending on the approximation chosen.

The linear spin density wave in Cr is characterized by an amplitude $\mu = \alpha_s g(T)$, a period a/δ and a phase θ. For $\vec{Q}_{\pm}$ oriented along the [001] direction the SDW can be written as [21]:

$$\vec{\mu}(z) = \vec{m}\alpha_s g(T)(-1)^{2z/a} \cos\left(\frac{2\pi}{a_{Cr}}\delta z - \theta\right) = \vec{\mu}_{Cr}(T)(-1)^{2z/a} \cos\left(\frac{2\pi}{a_{Cr}}\delta z - \theta\right) \tag{5}$$

where α_s is a constant amplitude, $g(T)$ is a normalized and temperature dependent order parameter, $\vec{m}$ is a unit spin polarization vector appropriate for longitudinal or transverse polarization and z $(= a/2, a, 3a/2, \ldots)$ is an index for the sequence of (001) lattice planes. For bulk Cr, the amplitude at zero temperature is $\mu(0) = \alpha_s g(0) = 0.5\ \mu_B$/atom. In neutron scattering experiments the Fourier transform of the SDW is determined. For a purely sinusoidal modulation of the spin lattice, only one harmonic occurs for each reciprocal lattice point with an intensity $I(\vec{Q}_{\pm})$ proportional to the square of the ensemble averaged SDW amplitude:

$$I(\vec{Q}_{\pm}, T) \propto \langle \vec{\mu}_{Cr}(T) \rangle^2 \tag{6}$$

and a position of the magnetic Bragg peak determined by the magnitude and orientation of the ordering wave vector $\vec{Q}_{\pm} = \vec{G}_{\{001\}}(1 \pm \delta)$ (see also section 4.1). Jiang and Fishman [16] maintain that the ordering wave vector $\vec{Q}_{\pm}$, as determined by neutron scattering, should be distinguished from the nesting wave vector $\vec{\Omega}_{\pm} = \vec{G}_{\{001\}}(1 \pm \Delta)$. $\vec{\Omega}_{\pm}$ measures the mismatch between the electron and hole Fermi surface, which in turn can be tuned continuously by alloying. For pure Cr at zero temperature $\Delta \approx 0.05$, which is bigger than $\delta \approx 0.04$. As Δ decreases continuously by alloying and the nesting between electron and hole Fermi surface improves, the SDW ordering wave vector may jump discontinuously to commensuration $\vec{Q}_{\pm} = \vec{G}_{100}$ with $\delta = 0$.

3.2. Surfaces

Early tight binding calculations of Allan showed for the first time that the Cr(001) surface would exhibit a magnetic moment of 2.8 μ_B, which is four to five times larger than in the bulk [22]. This finding has spurred a number of further theoretical investigations to study the surface magnetism of Cr. Subsequent theoretical work has to be divided into those considering the top layer of bulk Cr, a free standing Cr ML or Cr on ferromagnetic or paramagnetic substrates.

The magnetism of the top layers of Cr was also examined by Grempel [23]. Using a tight binding approach, he finds surface ferromagnetic order stabilized by coupling to the

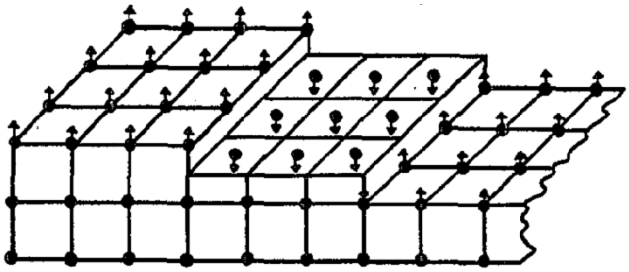

Figure 4. Magnetic order at the Cr(001) surface containing monatomic high steps. Each monolayer is ferromagnetically ordered and antiferromagnetically coupled to the next monolayer. On the terraced surface domains with opposite spin direction alternate, creating a topological antiferromagnet (from Blügel *et al* [26]).

bulk, a surface moment of 2.6 μ_B and a very high surface Curie temperature of about 800 K. Self-consistent tight binding calculations by Victora and Falicov [24] predict a giant spin polarization at the Cr surface of 3.0 electrons. Assuming an electronic g-factor of 2, this accounts to a Cr magnetic moment of 3 μ_B for the Cr(001) surface. *Ab initio* full-potential linearized augmented plane wave (FLAPW) calculations by Fu and Freeman [25] show that the surface enhanced magnetic moment is related to the sharp surface density of states peak near the Fermi level for the paramagnetic state. For the top Cr layer they find ferromagnetic order with a moment of 2.49 μ_B, whereas the first layer below the surface carries also an enhanced moment and is antiferromagnetically coupled to the surface layer with -1.29 μ_B. Blügel *et al* [26] considered surface magnetic structures other than the p(1×1) of Cr(001), but found this structure together with a layered antiferromagnetism along [001] the most stable configuration. On terraced surfaces with monolayer steps, ferromagnetic patches with opposite magnetization direction alternate, yielding a topological antiferromagnet, as sketched in figure 4.

Different from the Cr surface discussed above is the case of a Cr(001) monolayer on substrates other than Cr. This situation has been considered by Blügel *et al* [27] and Blügel [28] in the framework of density-functional theory applying the local density approximation. Specifically they have calculated the magnetism of a Cr(001) overlayer on a Pd(001) substrate. Using the bulk in-plane lattice parameter, they find an energy minimum for an antiferromagnetic c(2×2) structure with a local magnetic moment of 3.46 μ_B/atom. They assert that similar results are expected for Cr overlayers on Pt as well as on the noble metals Cu, Ag and Au. Slightly different is the case for one ML of Cr(001) sandwiched between Au(001). For this situation, Fu and Freeman [29] find an enhanced moment of 1.55 μ_B/atom, which is about half of that for a Cr overlayer on Au. Fu and Freeman interpret this result as being due to enhanced interface states near E_F, which become more delocalized by hybridization with the low lying Au d band as compared to the plain surface.

Highly interesting is also the case of a single isolated Cr(001) monolayer for which Blügel *et al* [27] find an antiferromagnetic c(2×2) structure and a local moment of 3.91 μ_B/atom. As soon as two more layers are added, Cr(001) develops a layered antiferromagnetic structure, i.e. the topmost layer has ferromagnetic p(1×1) structure with alternating spin orientation in the subsequent layers and lower local moment of 1.55 μ_B/atom.

Most theoretical investigations considering one or several ML of Cr deposited on a Fe(001) substrate find that Cr is ferromagnetically ordered with a p(1×1) structure. For one ML of Cr on Fe(100) an induced magnetization with a very large magnetic moment ranging from 3.1 to

3.65 μ_B /atom has been predicted to align antiparallel to the magnetization of the Fe substrate accompanied by a slight reduction of the interfacial Fe moment [24, 30]. More recent tight binding calculations by Vega *et al* [31] and Stoeffler *et al* [32] place the Cr magnetic moment between 2.5 and 3.2 μ_B. In contrast to previous work, the tight-binding calculations by Vega *et al* suggest that the c(2×2) structure might be energetically lower than p(1×1) for a Cr ML deposited on Fe(001). However, this would lead to spin frustrations at the Fe–Cr interface. A self-consistent tight binding calculation by Pizzagalli *et al* [33] finds that the most stable solution for an ML Cr on Fe(001) might be a ferrimagnetic order with a p(2×2) structure, which has been suggested previously by Victora and Falicov [24].

From the foregoing discussion the following conclusions can be drawn. The surface of Cr(001) exhibits an enhanced moment as compared to the bulk, is ferromagnetically ordered and is antiferromagnetically coupled to the subsurface layer. The magnetic moment enhancement decays rapidly within two or three layers beneath the surface. A free standing monolayer of Cr also exhibits an enhanced local magnetic moment, but in contrast to the surface layer it is definitely antiferromagnetically ordered with a c(2×2) structure. The same structure occurs for Cr(001) on (001) oriented Pd and Pt as well as on noble metal substrates. These properties stem from surface states with an increased density of states at the Fermi level. Details depend on the extent of delocalization due to hybridization effects with the substrate d band. The situation is different for a single Cr ML on Fe(001). Here the Cr layer is ferro- or ferrimagnetically ordered with a commensurate structure and antiferromagnetically coupled to the Fe substrate. The Cr moment is induced by proximity to the Fe substrate and exhibits an enhanced moment, which may be slightly lower than for the free standing film or for Cr on paramagnetic substrates, while the first Fe layer covered by Cr experiences a slight moment reduction. All these predictions are made for perfect surfaces and interfaces. However, Stoeffler and Gautier [32] have also considered the effect of roughness on the local magnetic moment distribution, which will be discussed later in subsection 3.4.

3.3. Thin films

For bulk Cr theory ascribes the formation of a SDW to the nesting between parallel sheets of the electron and hole Fermi surfaces, resulting in a lowering of the energy by opening a pseudo-band-gap at the Fermi surface. In layered systems with a broken symmetry in the direction normal to the film and limiting thickness it is *a priori* not clear whether the same mechanism works for the formation of a SDW as in the bulk. Furthermore, in thin films interface exchange and hybridization effects may have an important effect on the amplitude and wave vector of the SDW. Thus we expect that the difference between Cr thin films and bulk is determined by symmetry, proximity and finite size scaling.

Starting in the spirit of the previous paragraph we consider a number N of Cr(001) ML on an Fe(001) substrate. The first Cr(001) ML is expected to be in-plane ferromagnetically ordered with a p(1×1) structure and out-of-plane AF coupled to the Fe substrate. The second Cr ML is again F ordered and AF coupled to the previous Cr ML, setting up a layered antiferromagnetic structure with a two ML period. For thicker Cr layers the first phase slip indicates a transition from the commensurate to an incommensurate SDW. While the first Cr ML is undoubtedly F ordered due to the proximity to the Fe substrate, the question arises whether the magnetic order in and out of plane can be sustained for several ML, or whether it decays fast with the number of ML before the intrinsic I-SDW order sets in for a critical number N_c of Cr MLs. Accordingly, theoretical considerations need to distinguish Cr order for $N < N_c$ and $N > N_c$, and for temperatures above and below the bulk Néel temperature. If N chromium MLs are embedded in between two ferromagnetic layers F_1 and F_2, the magnetic order of Cr

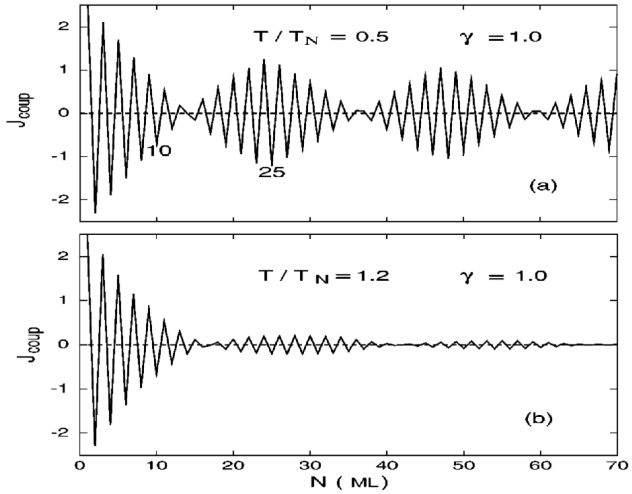

Figure 5. Oscillation of the exchange coupling reflecting the incommensurate spin density wave in Cr with a finite number of (001) oriented monolayers. On either side the Cr film is in contact with a ferromagnetic layer. (a) Spin density wave for $T = 0.5\ T_N$, (b) spin density wave for $T = 1.2\ T_N$ (from Shi and Fishman [36]).

may depend on whether the magnetization vectors in $F_{1,2}$ are aligned parallel (F-alignment) or antiparallel (AF-alignment) and whether the number of Cr MLs is even or odd.

The earliest theoretical study of Cr spin polarization on Fe(001) was carried out by Shi *et al* [34], following experimental observations by Unguris *et al* [35] of an I-SDW-like polarization in Cr for temperatures as high as 1.8 T_N. In a series of papers Fishman and Shi have systematically studied the SDW magnetism of a finite number of Cr monolayers sandwiched between Fe layers and using different boundary conditions [36–40]. First we discuss the case of a Cr spacer layer with thickness $L = (N-1)a/2$, collinearly coupled to proximity ferromagnetic layers on either side with moments $|\vec{\mu}_{F1}| = |\vec{\mu}_{F2}|$. The energy of the SDW per interface area a^2 can then be written [36]:

$$E = A[\vec{\mu}_{F1}\vec{\mu}_{Cr}(1) + \vec{\mu}_{F2}\vec{\mu}_{Cr}(N)] + \tfrac{1}{2}\Delta F a^3(N-1) \tag{7}$$

where A is an interfacial antiferromagnetic exchange coupling and ΔF is the nesting free energy per unit volume of the spacer at temperature T. The first term describes the proximity to the boundary layers and the second term the intrinsic instability of bulk Cr against the formation of an incommensurate SDW. For a temperature $T = 0.5\ T_N$ and with an increasing number of Cr(001) MLs, the magnetic coupling of the Cr layers oscillates with a 2 ML period. If the proximity magnetic layers are free to rotate between F ($\vec{\mu}_{F1} = \vec{\mu}_{F2}$) and AF alignment ($\vec{\mu}_{F1} = -\vec{\mu}_{F2}$), according to the number of Cr MLs in the spacer, the F configuration is stable for N odd, and the AF configuration is stable for N even between 1 and 24. Then the stability suddenly shifts to an even (odd) number between 24 and 39, and shifts again to an odd (even) number between 40 and 61. The exact location of the phase slips depends on the exchange parameters chosen. In any case, they indicate the appearance of nodes. For $N < 24$ the SDW order is commensurate; between 24 and 39 the Cr spacer contains one node, and between 40 and 61 two nodes. If the antinodes are located at the interface, one node is required for a half period SDW and two nodes for one complete SDW period. For $T = 1.2\ T_N$ the magnetic coupling shows almost the same periodicity, including the position of the nodes, but the amplitude quickly decays with thickness like $1/N^2$. Figure 5 shows the calculated shape

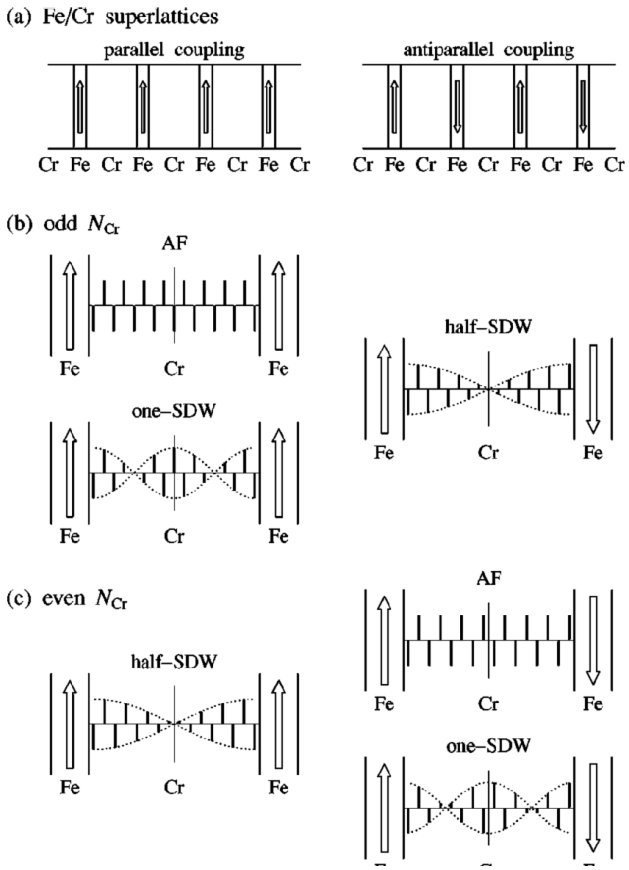

Figure 6. Spin structure in Cr films with an even and odd number of monolayers sandwiched between Fe layers. The Cr spin structure depends on the orientation of the Fe magnetization vectors and number of Cr monolayers. For N odd and Fe magnetization vectors parallel, the Cr spin structure is simple commensurate antiferromagnetic. Turning the Fe magnetization vectors from parallel to antiparallel, a node is induced in the Cr spin structure. For an even number of Cr monolayers the analogous situation occurs: commensurate antiferromagnetic spin structure for antiparallel Fe magnetization vectors and a node for parallel magnetization vectors. For the number of Cr monolayers below a critical number, all spin structures are commensurate with the Cr lattice. Spin structures shown are based on first principles calculations by Hirai [41].

of the SDW for Cr(001) sandwiched between Fe(001) layers and for temperatures below and above the bulk Néel temperature from the work of Shi and Fishman [36].

There is an important difference to be noted between I-SDWs in Cr films as compared to the bulk [36]. In thin films the period of the SDW is not as rigid and can easily deform to match the boundary conditions. For instance, 34 Cr MLs between two F aligned boundaries exhibit an enhanced amplitude and a single node in the centre. Adding successively two Cr MLs, this structure can be stretched up to 50 ML. However, adding two more MLs, the structure relaxes, two new nodes appear and the SDW amplitude drops towards the bulk value. As N increase further, the same stretching and relaxing starts again and the next jump takes place at 74 ML. For an odd number N of Cr spacer layers, the same cycle of stretching and relaxing is offset by 20 ML. This is a clear sign of proximity magnetism, maximizing the SDW amplitude at

the interface on one hand, and intrinsic I-SDW magnetism on the other hand, favouring bulk values for the SDW amplitude and wave vector.

So far we have considered proximity layers free to rotate in order to minimize the total free energy. If, on the other hand, the magnetization vectors $\vec{\mu}_{F1}$ and $\vec{\mu}_{F2}$ are controlled by an external field, the SDW order depends on their orientation and the number of Cr MLs in the spacer [36]. For instance, if N is even with $24 < N < 39$ and the boundary layers are F aligned, the resulting spin structure is an I-SDW with one node in the centre. Switching the $F_{1,2}$ layers to AF alignment, the Cr spin structure changes to C-SDW. Thus it is possible to switch between the I and C states by controlling the orientation of the magnetization vectors in the boundary layers.

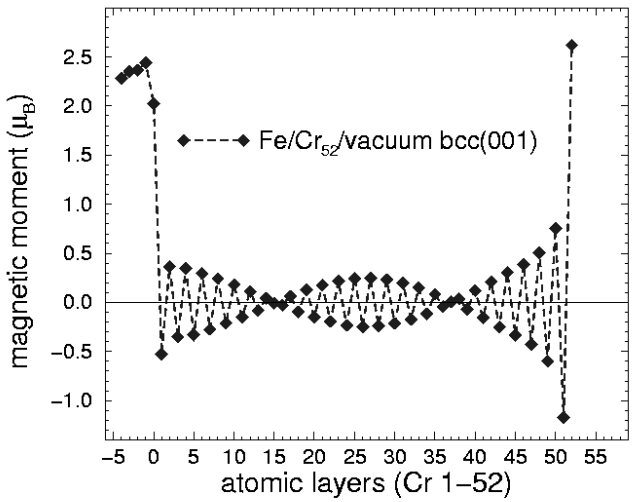

Figure 7. Calculations of the layer projected magnetic spin moments for 52 Cr monolayers sandwiched between Fe on one side and vacuum on the other side. The Cr monolayers in contact with Fe and vacuum exhibit an enhanced moment (from Niklasson *et al* [42]).

Recently first principles electronic-structure calculations for the SDW order in Fe/Cr/Fe superlattices have been presented by Hirai [41] which confirm the conclusions of Shi and Fishman. Hirai considers only Cr monolayers with $N < N_c \sim 24$. For an odd number N and F alignment of the Fe layers, the C-SDW is the stable configuration. With the same number N but switching the Fe layers from F to AF alignment places a node in the middle of the Cr layer and an antinode at the interfaces, hence producing half an I-SDW. For N even, the reverse is true. The spin structures for even and odd Cr monolayers and different alignments of the boundary F layers is reproduced in figure 6. Since the Cr spin structure is dictated by the boundary conditions, Hirai concludes that for $N < N_c$ the spin order is not a consequence of Fermi-surface nesting but is mainly governed by the boundary conditions, whereas intrinsic I-SDW is expected for a larger number of Cr MLs of at least $N = 19$.

Similar boundary conditions were considered by Niklasson *et al* [42] using the linearized muffin-tin-orbital method (LMTO) and the Greens' function technique. Their results are consistent with those of Shi and Fishman [36] and Hirai [41]. Niklasson *et al* have also calculated the SDW state of Cr in non-magnetic environments. For Fe/52 ML Cr/vacuum an I-SDW is obtained with a two ML periodicity and nodes at 15 and 36 ML, similar to the case of Fe/52 ML Cr/Fe. However, at the vacuum side the topmost Cr layer is ferromagnetically ordered with a surface moment of 2.6 μ_B/atom and an in-plane orientation which depends

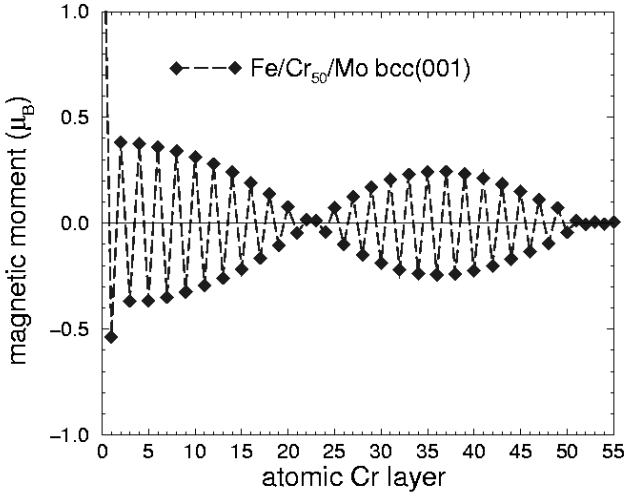

Figure 8. Similar calculations as in figure 7 but for a Cr film in contact with Fe on one side and Mo on the other side. On the Mo side a node in the Cr spin density is induced (from Niklasson *et al* [42]).

on N being even or odd. Therefore, at the Cr surface an anti-node exists always, as shown in figure 7. For 51 Cr MLs embedded in between Cu bcc(001) flats, antinodes occur at the Cu–Cr interface with an interface moment of 1.7 μ_B/atom and nodes at 15 and 37 ML. Since proximity magnetism is not at work for the presence of these nodes, they must be intrinsic, setting an upper limit for the appearance of intrinsic I-SDW in Cr. For Cr embedded between Fe and Mo, the Cr moment is enhanced on the Fe side, but quenched on the Mo side due to strong hybridization effects. Therefore on the Mo side a node is required (see figure 8).

The two monolayer periodicity, the surface and interface enhanced Cr moments at the vacuum and Fe side, respectively, and the rotation of the top Fe layer magnetization according to the number of MLs in the Cr spacer layer have already been noted by Stoeffler and Gautier using tight binding approximations [32]. The basic results obtained for $N \leqslant 10$ are in very good agreement with the latter first principles results.

Finally we need to discuss the dependence of the Néel temperature on the film thickness. Theory ascribes the finite size scaling of the critical temperature to the dimensional cross-over upon reduction of one of the linear dimensions [43]:

$$\frac{T_c(t) - T_c(\infty)}{T_c(\infty)} = \left(\frac{t}{t_0}\right) \tag{8}$$

where $T_c(\infty)$ is the bulk critical temperature, $T_c(t)$ the critical temperature for a finite thickness t and λ is the shift exponent related to the critical exponent ν for the correlation length according to

$$\xi = \xi_0 \left(\frac{T_c(t) - T_c(\infty)}{T_c(\infty)}\right)^{-\nu} \tag{9}$$

with $\nu = 1/\lambda$. For ferromagnetic films this type of scaling behaviour can indeed be observed [44]. However, for more complex spin structures with an extended repeat distance, the exact nature of scaling is still an open question. Fishman and Shi have addressed this question for the spin density waves in Cr [37, 40], where it is much more complex than for an elemental ferromagnet. On one hand the bulk Néel temperature is expected to scale with the thickness;

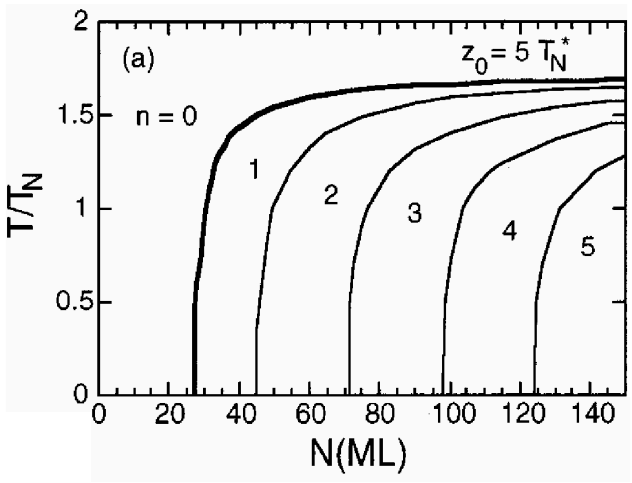

Figure 9. Dependence of the Néel temperature on the number of nodes n in the Cr film sandwiched between Fe boundary layers. The thick solid line denotes the phase boundary between commensurate and incommensurate spin structure while the thin solid lines separate regions for incommensurate phases with a different number of nodes n (from Fishman and Shi [40]).

on the other hand proximity to ferromagnetic boundaries stabilizes the SDW order in Cr spacer layers. Combining both effects, they find that the scaling of the Néel temperature depends on both the thickness of the Cr spacer layer t and the number of nodes n in the spacer: $T_N = T_N(N, n)$. Keeping n fixed, the Néel temperature drops to zero for a finite thickness $t_0(N, n) \approx na/2\delta$ as shown in figure 9. For a fixed temperature below T_N and an increasing number N of MLs, phase slips occur, whenever the scaling curve for a particular number of nodes is crossed. Between $n = 1$ and $n = 0$ an incommensurate–commensurate (IC) phase transition takes place, which according to figure 9 is the case for small $N < 24$ ML and/or high temperatures $T \geqslant 1.7\ T_N$. For low temperatures and fixed n the SDW period is almost constant. However, above T_N the period can be dramatically stretched before it undergoes an IC transition.

All calculations inherently assume that the interface exchange coupling between the in-plane magnetization of the ferromagnetic layers and Cr is strong enough to control the spin structure in Cr. As a consequence the spins in Cr are aligned either parallel or antiparallel to the in-plane magnetization of the ferromagnetic layer, setting up a single, linearly polarized and transverse SDW, with $\vec{Q}$ perpendicular to the film plane. According to Hirai [41], the helical or spiral SDW is never the more stable spin configuration as compared to the linear SDW, if the boundary Fe layers are collinearly F or AF aligned. However, when the magnetization vectors of adjacent Fe layers are not collinear, there appears to be a possibility for a helical SDW order (H-SDW). This confirms early tight binding calculations by Stoeffler and Gautier [45] that an H-SDW could be stable with perfect Fe/Cr interfaces but with non-collinear Fe magnetization vectors. On the other hand, the prerequisite for non-collinear Fe magnetization vectors is interface roughness, and this will be the topic of the next section.

From the foregoing discussion of finite Cr monolayers and proximity effects at perfect interfaces the following conclusions can be drawn:

(a) The interface between Cr and a noble metal will be similar to the Cr/vacuum interface and an enhanced moment can be expected for the next Cr layer closest to the interface due to surface or interface states. No proximity induced spin order occurs.

(b) At the interface between Cr and a ferromagnetic material, interfacial exchange coupling increases the magnetic moment, enhances the order parameter and changes the shape as well as the period of the SDW below the Néel temperature.
(c) Above the bulk Néel temperature, SDW order can be induced by proximity to a ferromagnetic layer. Although the SDW amplitude decays fast with increasing thickness, the nodes are reminiscent of the intrinsic I-SDW.
(d) At the interface between Cr and an early 4d or 5d transition metal, strong hybridization quenches the magnetic moment of Cr and places a node at the interface.
(e) In trilayers of F/N ML Cr(001)/F the SDW order depends on N and the collinear alignment of the F layers.
(f) For $N < 19$, C-SDW and I-SDW order is induced by the boundary conditions to the proximity layers. The I and C order can be switched by the F or AF alignment of the proximity boundary layers.
(g) For $N > 24$, a first intrinsic node appears, but the amplitude and wavenumber still depend on the boundary conditions. The I-SDW will stretch and collapse periodically as the Cr film increases in order to fulfil the boundary condition.
(h) For ferromagnetic boundary layers, in-plane magnetization, perfect interfaces and a small number of Cr layers, in-plane orientation of the Cr spins and a single linear and transverse SDW with $\vec{Q}$ oriented normal to the plane is the stable configuration.
(i) The Néel temperature scales with the film thickness and is a function of monolayers and nodes in the spacer.
(j) A helical SDW may only occur if the boundary ferromagnetic layers are non-collinearly aligned; otherwise the linear SDW is the more stable configuration.

While clear predictions exist for F/N Cr ML/F, the situation is less evident for Cr films embedded in a paramagnetic matrix. There is no *a priori* requirement for the Cr spins to align in the plane and to set up a transverse SDW with $\vec{Q}_{\pm}$ out of plane. The boundary conditions can also be fulfilled by a longitudinal SDW with an out-of-plane $\vec{Q}_{\pm}$, or by spin density waves oriented in the film plane. Spin flip transitions may occur and the coexistence of several domains is not excluded by the boundary conditions.

3.4. Rough interfaces

So far we have assumed ideal interfaces with a perfectly flat boundary. The effect of interface defects on the SDW state in Cr has been considered by a number of authors in recent years [32, 38, 40, 45–54]. First we need to distinguish between Cr/paramagnetic and Cr/ferromagnetic interfaces. At either interface the roughness may consist of single ion exchange, interdiffusion or alloying and steps with sharp terraces. In experiments one will certainly find a combination of these effects, but for a discussion of their action it is better to keep them separate.

Starting with the roughness at Cr/paramagnetic interfaces, single ion exchange is considered a weak defect which can be healed locally. For instance at Cr/Mo or Cr/Nb interfaces the Cr moment in the paramagnetic matrix will be quenched but spin frustration is excluded. Interdiffusion and alloying changes the magnetic properties of Cr, the ordering wave vector and the Néel temperature. Interface alloying will reduce T_N at the Cr/V interface and enhance T_N at the Cr/Mn interface. At the ideal Cr/Mo interface, a node of the I-SDW is required as shown in figure 8. Interdiffusion is expected to shift the node gradually away from the interface into the Cr matrix. At noble metal interfaces alloying will destroy the interface states and quench the moment enhancement. At surfaces alloying is not possible, but roughness

is expect to also destroy the surface states. Steps are not expected to cause frustration effects, since the layered antiferromagnetism of Cr is not altered.

At Cr/ferromagnetic interfaces the treatment of roughness is much more complex and many more possibilities exist to cope with the different types of defect. Single ion exchange causes a local non-propagating frustration. In case of interdiffusion two cases have to be distinguished. For a lower degree of interdiffusion, an antinode may still exist close to the interface, but the phase may be shifted by one monolayer, such that the second layer on top of an Fe substrate is antiferromagnetically instead of ferromagnetically coupled to the Fe substrate [32]. Freyss *et al* have determined the concentration for which a phase change occurs [54]. On the assumption that two monolayers at the interface are intermixed, a π phase shift occurs at a Cr concentration of 33%, whereas the phase changes at a 50% level if three monolayers are intermixed. For a larger degree of interdiffusion various theoretical treatments agree that the Cr moment becomes strongly reduced to the point that a node is placed at the interface [32, 40, 46, 53, 54]. For a Cr spacer layer embedded between two rough interfaces, SDW order requires the number of nodes in the spacer layer to be $n \geqslant 2$. No proximity enhanced order parameter at the interface is possible nor a commensurate structure for $N < 20$, since the nodes exclude commensuration. With increasing N the SDW will undergo a cycle of stretching and contraction as in the case of the perfect interfaces. Each time a node is added, the order parameter, period and Néel temperature exhibit a jump. For large N, these properties approach their bulk values. For $N < 20$ ML the Néel temperature drops to zero since N is less than required for half an SDW period and since C-SDW order cannot gain any coupling energy due to lack of contact with the proximity layers [40].

While steps at the Cr/paramagnetic interface are harmless, they constitute the single most severe defect at the Cr/ferromagnetic interface. The response to this defect depends on the terrace length, the Cr and Fe layer thicknesses and their respective exchange coupling constants. Many different scenarios can be visualized, including domain formation in the Fe layer, in the Cr layer or non-collinear magnetization vectors in successive ferromagnetic layers along with a helical twisting of the Cr spin structure. For a Cr thickness large compared to the average terrace length, the ordering wave vector $\vec{Q}_{\pm}$ is likely to rotate from perpendicular to in plane.

Stoeffler and coworkers [32, 45, 46] have considered different situations for domain walls in Cr propagating to the surface or being confined to the area around the step, as shown schematically in figure 10. Assuming a straight domain wall, the defect energy stored depends linearly on the Cr thickness as $E_{Def} = \mu_{Cr} + \gamma_{Cr} t_{Cr} + \sigma_{Cr}$, where μ_{Cr} and σ_{Cr} are interface and surface contributions to the defect energy, respectively, and γ_{Cr} is the energy per in-plane Cr atom in the domain wall. The energy can be lowered if a domain wall connects two successive steps at distance λ. In this case the defect energy is $E'_{Def} = \mu_{Cr} + \gamma_{Cr}\lambda$, which becomes smaller for a Cr layer thickness exceeding $\lambda/2 - \sigma_{Cr}/\gamma_{Cr}$. Estimates of the ratio σ_{Cr}/γ_{Cr} yield a critical thickness of $t_{Cr} > \lambda/2 - 10$ ML for which the domain wall becomes localized close to a kink. Typical terrace widths for high quality epitaxial growth are about 300 Å, such that localization is expected for thicknesses larger than 140 Å. If the Cr film is covered with another ferromagnetic layer, the domain walls have to accommodate the step structure at the lower as well as at the upper interface. Localization of the domain walls by connecting steps at the same interface may again take place under conditions mentioned before, shielding the remaining layer from the defect area [46].

Berger and Fullerton [47] have employed a local Ising model solved in the mean field approximation to study frustration effects at kinks. Similar to the results of Stoeffler *et al* [32, 45] they establish a phase diagram as a function of Fe and Cr layer thickness and of temperature for propagating domain walls in Cr from the interface to the surface, in the Fe

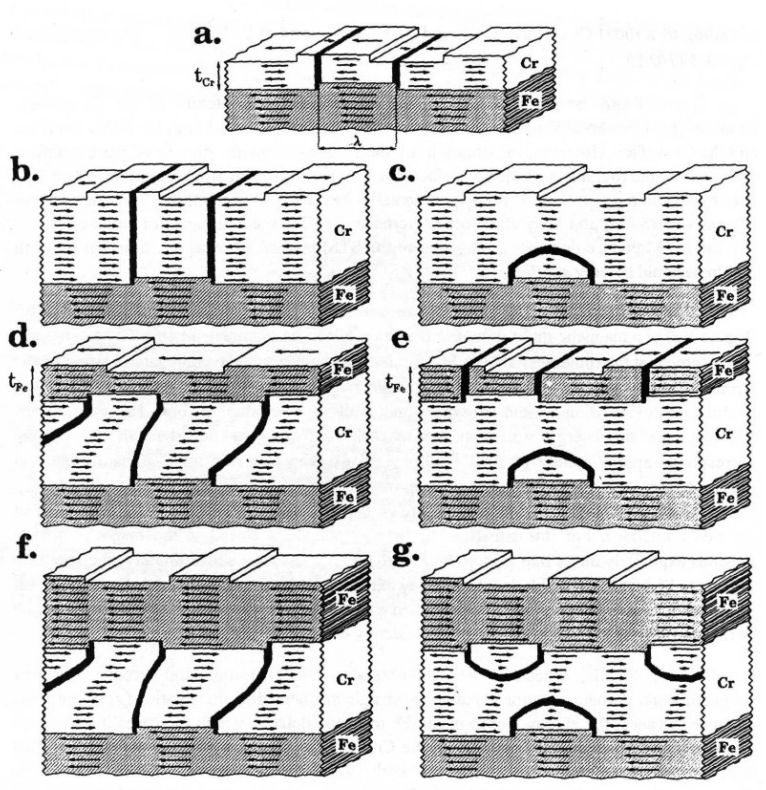

Figure 10. Schematic representation of several possibilities for interface roughness at the Fe/Cr interface, according to Vega *et al* [46]: (a) initial stage of growth of Cr on a rough Fe surface with the possibility of domain formation in the Cr layer; (b), (d), (f) the case for thin Cr films, (c), (e), (g) the case for thick Cr layers compared to the step separation λ. (b) continuation of (a) with straight domain walls in the Cr layer; (d) domain bending by connecting steps on either side of rough interfaces without domain formation in the Fe layer; (f) continuation of (d) with increasing Fe thickness; (c) localization of the domain in the Cr layer to the interface by connecting two successive steps at distance λ; (e) growth of thin Fe layer on a rough Cr surface results in domain formation in the Fe layer; (g) with increasing Fe thickness, the top Fe layer forms a single domain and the frustrations in the Cr film become localized at the interfaces.

layer and for confinement of the domain wall to the interface. In contrast, Bödeker *et al* [48] and Hucht [49] use a local Heisenberg model together with a single ion anisotropy term for modelling the spin structure in Fe and Cr with frustration effects at the interface. In the case of a step at the interface it is no longer possible to minimize all three coupling energies, J_{Fe-Fe}, J_{Cr-Cr} and J_{Fe-Cr}, independently. Thus, the resulting spin structure of the system depends on the values of the respective coupling constants. The following four limiting cases, which are sketched in figure 11, can be distinguished assuming a single monatomic step at the interface. If the interface coupling J_{Fe-Cr} is large compared to J_{Fe-Fe} and J_{Cr-Cr}, a domain wall forms in the Fe layer (case (c)), or in the Cr layer (case (d)). For a very small interface coupling J_{Fe-Cr}, the ideal FM and AF order in the Fe and Cr layers can be preserved by a domain wall forming along the interface (case (b)). If, however, the AF interface coupling is of intermediate magnitude, the system can react by reorienting the Cr moments perpendicular to the Fe (case (e)). This phenomenological

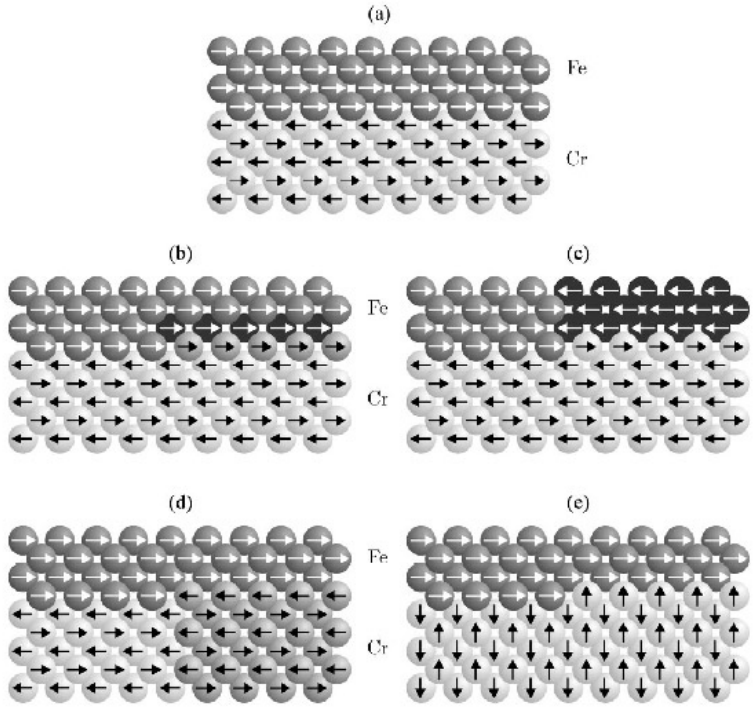

Figure 11. Schematic and simplified representation of the interface between a thin ferromagnetic Fe layer and a thicker antiferromagnetic Cr film. The white arrows indicate the orientation of the magnetic moments in the Fe film, the black arrows the Cr magnetic moments. (a) An ideal and flat interface with antiferromagnetic coupling between the Fe and Cr moments. (b)–(e) Interfaces with monatomic high steps causing frustration of the interface exchange coupling. The frustration can be overcome by formation of a domain in the Fe layer (c) in the Cr film (d) or by a reorientation of the spin-density wave (e). The latter case is observed experimentally in thick Cr films (from Bödeker *et al* [56]).

description is confirmed by computer simulations of a classical Heisenberg model taking into account nearest-neighbour interaction and a single ion anisotropy term to model the shape anisotropy. In figure 12 the resulting ground state spin configuration is shown. As one can readily see, the frustration induces an effective 90° rotation of the Cr moments at some distance to the interface, while close to the interface the antiferromagnetic coupling is preserved to a large extent. Macroscopically this rotation leads to a perpendicular orientation of the Cr spins with respect to the Fe in-plane magnetization. For a transverse I-SDW the wave vector is then expected to lie in the plane, consistent with experimental observation for a thickness range large compared to the average distance L between steps [48]. A crossover from out-of-plane to in-plane spin orientation takes place roughly when the condition $J_{Cr-Cr}t_{Cr} = J_{Fe-Cr}L$ is fulfilled. If J_{Cr-Cr} and J_{Fe-Cr} are of the same order of magnitude, this will occur for a Cr thickness equalling the average distance between monatomic steps.

With intermediate disorder, such as steps separated by large terraces, the coupling between an I-SDW and proximity layers is reduced but not extinct. Fishman [38] has calculated the magnetic phase diagram for steps at the Fe/Cr interface and finds that for a small Cr thickness or for a high temperature a helical SDW is stabilized by the interfacial coupling. However,

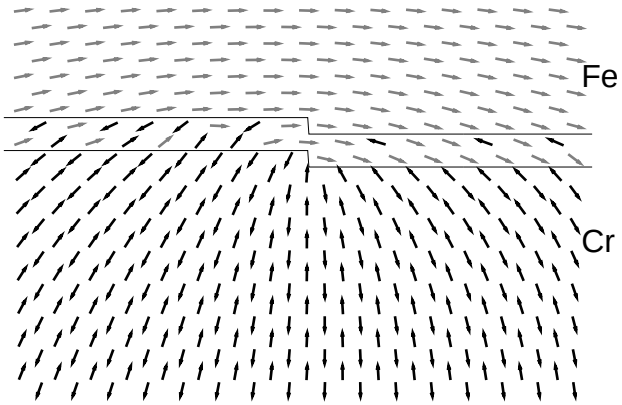

Figure 12. Ground state spin structure near an Fe/Cr interface with a monatomic step from computer simulations based on a Heisenberg model assuming interdiffusion over two layers. On either side of the step the Cr moments try to align antiparallel to the Fe moments. The combined action is a rotation of the magnetic moments from parallel to perpendicular orientation with respect to the in-plane magnetization of the Fe film. Note that the Fe moments are also affected (from Bödeker *et al* [48]).

only helical order with a single twist of $\pm\pi/2$ is stable; higher order helices may be frustrated by the presence of defects. The helical spin order between non-collinear Fe magnetization vectors is shown in figure 13 [38]. With decreasing temperature I-SDW and H-SDW order may coexist. Slonczewski has already argued that in the presence of steps at the Fe–Cr interface, non-collinear orientations of the adjacent Fe magnetization vectors may occur, mediated by the intervening Cr spins which are twisted counter-clockwise on either side of a step [50, 51]. In the proximity magnetism model the exchange coupling energy of the adjacent Fe layers is expressed phenomenologically as:

$$E = -J_- \left(\frac{\theta}{\pi}\right)^2 - J_+ \left(\frac{\theta - \pi}{\pi}\right)^2 \tag{10}$$

with $0 \leqslant \theta \leqslant \pi$. The coupling constants J_- and J_+ favour ferromagnetic ($\theta = 0$) and antiferromagnetic ($\theta = \pi$) coupling for perfect interfaces with N odd or even, respectively. The competition between the two results in a non-collinear 90° orientation of the successive Fe layers if $|J_-| = |J_+|$, but can deviate from 90° for different J_- and J_+ values. Freyss *et al* [52] have performed band structure calculations to determine self-consistently the magnitude and orientation of the Fe and Cr moments in case of non-collinear Fe coupling. They find that for more than five Cr MLs the phenomenological expression by Slonczewski for the exchange coupling energy is satisfied, but deviations occur for smaller numbers because of moment reduction at the interface and perturbation of the collinear order within the Fe layer.

The effect of roughness can clearly be classified into three categories. In the first category belong almost ideal interfaces with random ion exchange, causing a partial alloying. The main effect of the alloying is to shift the phase of the interface exchange coupling by π, such that at a distance of two Cr MLs away from the interface the Cr magnetic moment is antiparallel to the Fe magnetization vector instead of parallel, as one would expect for an ideal interface. With increasing roughness a node is expected at the interface. In this case the SDW cannot take any advantage of the proximity magnetism to the F layer and I-SDW order should first occur

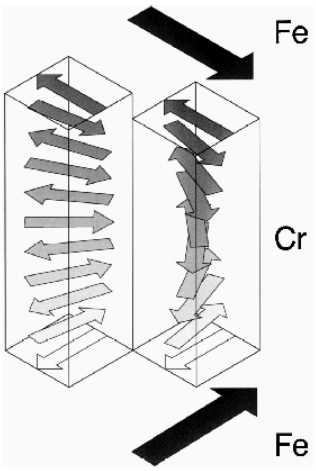

Figure 13. A sketch of two commensurate and twisted (helical) SDW, one right handed with 11 monolayers and the other left handed with 10 monolayers, coupling Fe moments 90° apart due to a step at the interface. At the interface the Fe and Cr moments are antiparallel (from Fishman [38]).

if two nodes on either side of the interface fit within the Cr spacer thickness for appropriate temperatures. With increasing roughness the interface may develop spin glass properties and the node may shift some distance away from the interface. Steps with flat terraces between them belong to the third category. For a Cr film thickness larger than the average step separation, a reorientation of the SDW wave vector from perpendicular to the plane to in plane can occur. For a smaller thickness, the orientation of $\vec{Q}_{\pm}$ remains perpendicular and the domain becomes localized close to the kink. This a clear idealization of the real situation, since alloying will also occur on the terraces.

4. Experimental techniques

In the following a few experimental techniques are recalled, which are capable of determining directly the SDW order in Cr. These are neutron scattering, x-ray scattering and perturbed angular correlation spectroscopy. All other methods, which have been used in recent years for unravelling the Cr order, are more indirect and rely on the interface exchange interaction between a ferromagnetic cap layer on Cr, measuring either the ferromagnetic hysteresis or the domain structure in the ferromagnetic film. Another class of experiments uses surface sensitive and polarized probes such as spin polarized secondary-electron emission (SPSEE), spin resolved core level photoemission spectroscopy, spin polarized electron-energy loss spectroscopy (SPEELS) etc. These methods will not be reviewed here but will be mentioned along with a discussion of the corresponding experiments.

4.1. Neutron scattering

The sinusoidal modulation of the magnetic moments produces sharp Fourier components in the reciprocal lattice, which can most effectively be determined by elastic neutron scattering [1, 11]. With this method the spin orientation and the propagation direction of the spin density waves can be analysed. Furthermore, commensurate and incommensurate SDW order can easily be distinguished and the magnetic moments including their orientation can be determined. In neutron scattering experiments the magnetic moment of the neutrons couple to the magnetic moments of the magnetic material via dipolar interaction. Working out the elastic scattering

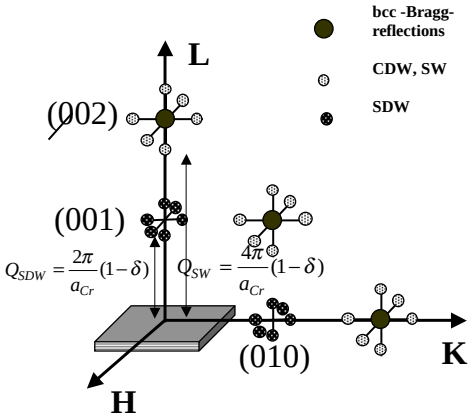

Figure 14. Partial reciprocal lattice showing the positions for the satellite reflections due to spin density waves and strain waves in Cr. The L direction is chosen to be perpendicular to the film plane. The SDW satellite positions are denoted by open circles, the SW satellite positions by filled small circles. The large dots denote allowed bcc reflections.

cross section, one obtains for the scattering cross section of an unpolarized neutron beam with the spin density wave $\vec{\mu}(\vec{Q}_{\pm})$ [6, 55]:

$$\left(\frac{\mathrm{d}\sigma}{\mathrm{d}\Omega}\right)_{el,mag} = |\vec{\mu}_{\vec{K}}|^2 \sin^2(\Phi_{\vec{K}})\delta(\vec{K} + \vec{Q}_{\pm} - \vec{G}_{bcc}) \tag{11}$$

where Φ_K is the angle between the magnetization $\vec{\mu}$ and the scattering vector $\vec{K}$ ($|\vec{K}| = (4\pi/\lambda)\sin\theta$), $\vec{Q}_{\pm} = \vec{G}_{\{001\}}(1-\delta)$ is the wave vector for the SDW, $\vec{G}_{bcc}$ are the reciprocal lattice vectors for allowed bcc reflections and $\vec{\mu}_K$ is the Fourier component of the magnetization vector $\vec{\mu}(\vec{r})$ corresponding to the scattering vector $\vec{K} = \vec{k}' - \vec{k}$. The delta function warrants that intensity occurs only at positions in the reciprocal lattice for which the scattering vector fulfils the condition: $\vec{K} = \vec{G}_{bcc} \pm \vec{Q}_{\pm}$.

Figure 14 shows a partial reciprocal lattice for Cr. The SDW satellite peaks are marked by open circles. They occur around the structurally forbidden bcc reflections. Any intensity in their vicinity has therefore to be of magnetic origin. There are two selection rules to be obeyed for determining $\vec{Q}_{\pm}$ and $\vec{\mu}_{\vec{K}}$. First, the vector connecting a satellite peak with the nearest allowed reciprocal lattice point $\vec{G}_{bcc}$ along any one of the {100} directions determines the orientation and magnitude of $\vec{Q}_{\pm}$. Second, the magnetic neutron scattering cross section yields intensity only for components of $\vec{\mu}_{\vec{K}}$, which are perpendicular to the scattering vector $\vec{K}$. Scans around a few orthogonal reciprocal lattice points uniquely determine the orientation and polarization of the SDW [14, 56]. For example, satellite peaks parallel to the [001] direction on either side of the (001) position reveal an out-of-plane transverse SDW with spins either pointing in the [100] or [010] direction. Satellite reflections around the (010) position in the [001] direction indicate again an SDW with $\vec{Q}_{\pm}$ out of plane, but either with longitudinal or with transverse character. Several scans are usually required to uniquely determine the polarization of the SDW and all possible volume fractions of coexisting domains. In addition, with neutron scattering it is easy to detect any commensurate SDW phase, since this generates a peak at the structurally forbidden $\vec{G}_{\{100\}}$ positions.

4.2. X-ray scattering

Scattering with synchrotron x-ray photons is a very important alternative to neutron scattering. The spin density wave sets up a charge density and a strain wave with wave vector $2\vec{Q}_{\pm}$ in the Cr lattice. The amplitude of the charge density wave is very small and can hardly be recognized. The strain wave, on the other hand, is easier to detect. The Thomson cross section for the strain waves is given by [57]:

$$\left(\frac{\mathrm{d}\sigma}{\mathrm{d}\Omega}\right)_{x-ray} = \frac{1}{4}|\rho_0(\vec{K})(\vec{K}\,\vec{\Delta})|^2\delta(\vec{K} \pm 2\vec{Q}_{\pm} - \vec{G}_{bcc}) \tag{12}$$

where $\vec{\Delta}$ is the strain wave amplitude and ρ_0 is the average electron density. The delta function expresses the fact that the strain wave vector is doubled compared to the SDW. Thus the satellite peaks from the SW occur close to the structurally allowed reciprocal lattice points $\vec{G}_{bcc}$, as indicated by the shaded dots in figure 14. The SW can be visualized as a frozen phonon modulating the lattice in the direction parallel to $\vec{Q}_{\pm}$, yielding the same selection rule for the scattering cross section as a one phonon cross section. Because of the scalar product $(\vec{K}\,\vec{\Delta})$, only the SW with $\vec{Q}_{\pm}$ parallel to the scattering vector $\vec{K}$ produces intensity; the others are silent. Thus from the Thomson scattering follows the orientation of the SDW; the polarization cannot be determined. The SW satellite peaks were first observed with x-rays by Tsunoda *et al* [58]. Using high resolution x-ray scattering with synchrotron radiation, Gibbs *et al* determined the temperature dependence of the $2\vec{Q}_{\pm}$ peak [12]. An extensive synchrotron radiation study of the SW satellite peaks including their temperature dependence was carried out recently by Hill *et al* [13].

With synchrotron radiation of incident photon energy of $E = 5.91$ keV, which is just below the Cr K edge, satellite peaks at the $\{1 \pm \delta, 0, 0\}$ positions have been observed, which are of magnetic origin [13]. The magnetic intensity is, however, non-resonant and therefore too weak to be of practical interest for thin film studies.

Investigations of the magnetic order in Cr via the strain wave vector $2\vec{Q}_{\pm}$ takes advantage of the high intensity of synchrotron sources as compared to neutron sources. Therefore this method can also be applied to thin films. The first investigation of thin Cr film via synchrotron radiation was published by Sonntag *et al* [59]. The method is limited by the high background at the $2\vec{Q}_{\pm}$ position due to the adjacent charge peak at $\vec{G}_{bcc}$. With increasing temperature the situation becomes worse, since $2\vec{Q}_{\pm}$ increases and the satellite peaks move closer towards the charge peak. In contrast to neutron scattering, with x-ray scattering the AF_0 phase cannot be detected, since the commensurate peak is completely covered by charge scattering.

4.3. Perturbed angular correlation spectroscopy

The method of perturbed angular correlation spectroscopy (PACS) has recently been used for the first time by Meersschaut *et al* [60] to study the spin density wave magnetism in thin Cr films. The β^--decay of ^{111}In (^{111}Cd) isotopes implanted in the film is followed by a γ–γ cascade of ^{111}Cd, which is detected by two oppositely placed counters. In the coincidence experiment the time correlation between the two γ particles is determined. Since the radioactive nuclei are embedded in the hyperfine field of the host matrix, they will precess about the main field axes. The γ–γ emission is axially symmetric about the direction perpendicular to the hyperfine field. After emitting the first γ ray, the time dependent anisotropy of the second γ ray reflects the Larmor frequency, which in turn is proportional to the strength of the hyperfine field. For a ferromagnet or a commensurate antiferromagnet the PAC time spectrum consists of one or two damped cosine terms for the ground frequency and its first harmonic. In case of an incommensurate and sinusoidally varying hyperfine field, the PAC time spectrum is determined

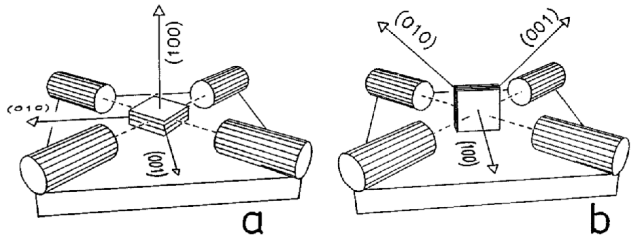

Figure 15. Schematic view of the configuration of the detectors and the sample (a) in the perpendicular geometry and (b) in the in-plane geometry used in perturbed angular correlation spectroscopy experiments (from Meersschaut *et al* [60]).

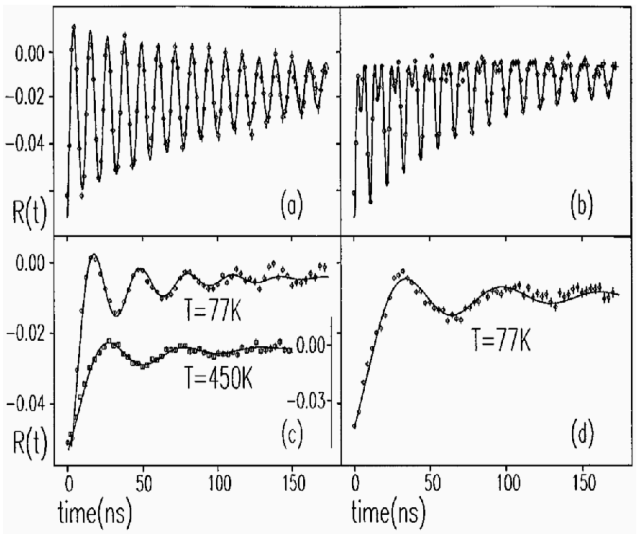

Figure 16. The top panels (a) and (b) show reference PAC time spectra for a 38 nm Fe film, grown on MgO, taken at 289 K, perpendicular (a) and in-plane geometry (a), as defined in figure 15. The solid lines are fits to the data using the first sum in equation (13). In the lower panels are shown the PAC time spectra for a 20 Å Fe/400 Å Cr heterostructure grown on an MgO(001) substrate taken in the perpendicular (c) and in-plane (d) geometry. The solid line corresponds to an incommensurate SDW, described by the second sum in equation (13) (from Meersschaut *et al* [60]).

by a Overhauser distribution of hyperfine fields, yielding one or two damped Bessel functions of zeroth order. For both cases the time correlation function can be expressed as [60–63]:

$$R(t) = f_{CSDW} \sum_{n=0,2} a_n \, \mathrm{e}^{-n\delta\nu_C t} \cos(n\nu_C t) + f_{ISDW} \sum_{n=0,2} b_n \, \mathrm{e}^{-n\delta\nu_I t} J_0(n\nu_I t) \tag{13}$$

where f_{CSDW} and f_{ISDW} are the relative fraction of the C-SDW and I-SDW phases, ν is the Lamor frequency proportional to the local hyperfine field and J_0 is the Bessel function of zeroth order.

The interpretation of the PAC time spectra relies on the fact that the hyperfine field and the Cr moments are collinear. If the hyperfine field is perpendicular to the detector plane consisting of four detectors separated by 90°, as shown in figure 15, a double frequency is observed, whereas if the hyperfine field lies in the detector plane only one frequency is visible.

Thus, the orientation of the hyperfine field relative to the detector plane is uniquely determined by two orientations of the sample with respect to the detector plane. A typical example is shown in figure 16. This method is therefore capable of detecting the magnetic state in Cr films and of distinguishing between commensurate, incommensurate and paramagnetic phases. Furthermore, the PAC technique has the advantage of being sensitive to the absolute volume fraction of any coexisting phases and to their simultaneous magnetic moments. However, it does not yield information on the orientation of the ordering wave vector. Therefore it is not possible to distinguish between L-SDW and T-SDW. On the other hand, the hyperfine field value depends on the polarization of the SDW, being larger for longitudinal polarization than for transverse. Therefore the hyperfine field value provides an indirect indication even for the polarization of the SDW [63].

Mössbauer spectroscopy is an alternative method to perturbed angular correlation spectroscopy, yielding information on hyperfine fields, magnetic order and anisotropy. However, there is no Cr isotope which could be used as a nuclear probe. Therefore, all information about Cr is indirect from either implantation of nuclear probes or by Mössbauer active isotopes in adjacent layers. Obviously, ^{57}Fe is the isotope of choice. However, in this case the ferromagnetism of Fe is probed more than the antiferromagnetism of Cr, since the hyperfine field of the surrounding Fe atoms is stronger than the hyperfine field from the distant Cr film [64]. An exemption is the ^{119}Sn isotope, which has also been used as a Mössbauer probe in paramagnetic Sn layers. In this case a hyperfine field distribution can be detected even at some distance to the antiferromagnetic Cr layers [65, 66].

5. Experimental results

5.1. Growth studies of Cr

Because of the exciting theoretical predictions concerning the magnetism of single Cr layers and superlattices containing Cr spacer layers, a substrate for perfect and uniform epitaxial growth of single Cr films is in high demand. A number of substrates have been tested for Cr growth with different success, including Al, V, Fe, Co, Cu, Ag, Nb, W and Au. Furthermore, Cr has been grown on semiconductor substrates such as Si and GaAs, and on insulator substrates LiF and MgO. The growth of thin epitaxial films is reviewed by E Bauer in this volume [67]. Therefore only some specific cases will be considered here.

Because of the very good lattice match between Cr on Ag(001) and Au(001), these surfaces would be ideal candidates for layer by layer growth. However, Cr on Au(100) shows a tendency for alloying at the interface (Hanf *et al* [68]) and Cr on Ag(100) exhibits a tendency of island growth even in the submonolayer region and at room temperature (Krembel *et al* [69]). After a coverage of 4–5 ML, the Cr film resembles more that of a bulk Cr surface.

Sonntag *et al* [70] have studied to some extent the MBE growth of Cr(110) on Nb(110)/$Al_2O_3(11\bar{2}0)$. Cr(110) forms a single domain structure on Nb(110) and the lattices exactly align in the plane. The perpendicular coherence length of the Cr film is about 90% of the total film thickness, and the out-of-plane mosaicity is 0.6°, whereas the in-plane mosaicity ranges from 0.3 to 0.9°. The Nb buffer layer on the sapphire substrate is elastically relaxed and exhibits the intrinsic lattice parameter. Between Nb and Cr there is a lattice mismatch of 14%. With this large lattice mismatch one should expect that the Cr lattice relaxes within the first few monolayers. Contrary to expectations, the elastic relaxation of the Cr films turns out to be quite unusual. While the in-plane lattice relaxes with increasing film thickness towards the bulk lattice parameter in the expected way, the out-of-plane lattice parameter does not exhibit a corresponding Poisson response. Instead the Cr out-of-plane lattice parameter maintains its

bulk value for all thicknesses independent of the in-plane relaxation. It was speculated that there is a correlation between the single domain longitudinal SDW for Cr(110) films on Nb and the anomalous elastic behaviour.

Bödeker *et al* [56] have studied in detail the MBE growth of Cr(001) on Al_2O_3 $(1\bar{1}02)$ with an Nb(001) buffer layer, using RHEED, LEED, Auger and x-ray analysis. At the optimized growth temperature of 450 °C a layer-by-layer growth was observed with essentially no increase of the surface roughness. Post-growth annealing improves further the surface quality and structural coherence of the Cr film. The out-of-plane structural coherence lengths comprise typically 50–80% of the total film thickness, whereas the in-plane structural coherence lengths lie between 250 and 350 Å. The out-of-plane and in-plane mosaicities are 0.2–0.3 and 0.3–0.4°, respectively, which is slightly better than for Cr(110) films. The epitaxial relationship between Cr(001) and Nb(001) is such that the {100} axes of both metals are parallel.

Cr growth on W(100) and W(110) should be comparable to the growth on Nb(100) and Nb(110). The difference is a smaller lattice mismatch in the former system (9%) as compared to the latter (14%). Berlowitz and Shinn [71, 72] have studied the Cr growth on W from the monolayer range up to a couple of monolayers. While layer-by-layer growth and pseudomorphic (1×1) structures are observed on both substrate orientations at 100 K with a stability of up to about 1300 K, thicker films show the Stranski–Kastranov growth mode forming three dimensional clusters on top of the pseudomorphic Cr/W monolayers. At the same time the thermal stability of the layer is much reduced to about 400–500 K. The desorption experiments showed that the bonding of Cr on both W substrates is stronger than Cr to itself. The same workers also noted that there is an interesting variance in the work function behaviour for Cr/W as compared to other metal overlayers in that there is little difference between the work function of one ML Cr on W and the work function for bulk Cr. This appears to reflect a subtlety in the charge transfer between W and the top Cr layer and could also have an effect on the boundary conditions for the SDW at the Cr/W interface as soon as it emerges in thicker Cr layers.

Cr growth on LiF(001) has been studied in detail by Mattson *et al* [73]. The optimal growth conditions are cited as 400 °C. At this temperature, Cr first grows in a mixed mode followed by a layer-by-layer growth beyond 200 Å.

Cr and Al are both bcc metals with a fairly small lattice mismatch of only 0.7%. Thus, from a misfit point of view, Cr should grow well on Al. On the contrary, Kim *et al* [74] showed that already a fraction of a monolayer of Cr on Al(001) leads to an immediate loss of the LEED pattern, destroying even the crystalline structure beneath the surface. Continued deposition restores the Cr structure, which appears to have the same orientation as the Al substrate, although film and substrate are separated by a disordered interface a couple of monolayers thick.

Cr growth on Co(0001) is different from the heteroepitaxial systems mentioned before, because of the different symmetries. Ohresser *et al* [75, 76] find that the growth of Cr on Co(0001) strongly depends on the substrate temperature. At room temperature a layer-by-layer growth mode is observed with a Nishiyama–Wassermann epitaxial relationship, while at higher temperatures the interface becomes diffuse and epitaxial islands form with Kurdjumov–Sachs epitaxial orientation.

Metoki *et al* [77] have studied the growth of Co/Cr(001) superlattices. When starting with the growth of Co on Cr(001), Co grows pseudomorphically with a pseudo-bcc structure, which relaxes back to the intrinsic hcp structure after deposition of about 40 Å. Then the [0001] axis lies in the film plane parallel to the Cr[110] axis. Deposition of Cr on this Co surface leads to a sudden relaxation of the pseudomorphic Cr structure to bulk-like bcc after deposition of 5 ML.

Investigations of Cr growth on Fe and vice versa is most important as these interfaces have model character for testing theories concerning exchange coupling effects and the intrinsic

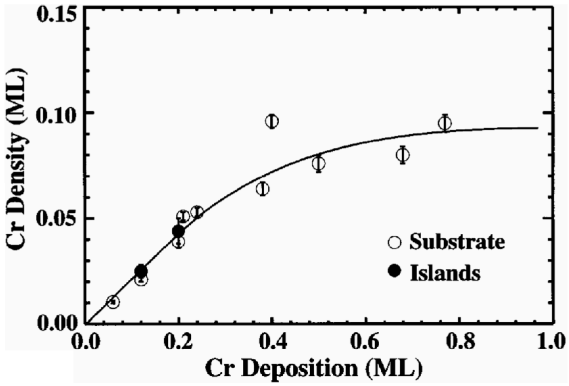

Figure 17. Plot of the Cr concentration in the surface layers versus Cr deposition for a growth temperature of 300 °C. The empty and filled circles represent the concentrations on the substrate and the first growth layer, respectively (from Davies *et al* [78]).

magnetic order of Cr. Although the growth of Cr on Fe should be almost ideal due to the close lattice match and the availability of nearly perfect, single crystal Fe(001) whisker substrates, experimental evidence tells us otherwise. Using scanning tunnelling microscopy and tunnel spectroscopy, Davies *et al* [78] have shown that under layer-by-layer growth conditions Cr deposition leads to the formation of a Cr–Fe alloy within the first few monolayers. At a growth temperature of 300 °C only one out of every four deposited Cr atoms remains in the surface layers; the others diffuse to subsurface sites. After completion of 1 ML Cr, only a fraction of about 0.10 ML resides in the surface layer, as shown in figure 17. The tunnelling spectroscopy measurements suggest that the first predominantly Cr layer occurs at a Cr coverage of no more than 2–3 ML. Interdiffusion also takes place below the surface and may go as deep as to the third layer below the surface, as indicated by angle-resolved Auger electron spectroscopy by Venus and Heinrich [79]. Cr growth on Fe whiskers has also been studied in detail by Pierce *et al* [80]. STM images after deposition of 5 ML of Cr at 50 °C show island growth with a mean square roughness of 0.86 ML. At 215 °C the island size has increased by a factor of 20 and the rms roughness is reduced to about 0.47 ML. At 300 °C true layer-by-layer growth is observed. On the other hand, Fe growth on Cr is much more perfect and interdiffusion is hardly recognized.

Cr growth on Cu(001) was investigated by Lawler *et al* [81] in the hope of finding a pseudomorphic fct phase. However, no indication for such a structure has been obtained even in the submonolayer region. The growth is found to be three dimensional in character with the formation of irregular multilayer high islands forming four equivalent domains. A number of studies with different methods assure that Cr retains its bulk bcc structure on Cu(001) [82–84].

5.2. Magnetism of Cr monolayers and surfaces

The magnetism of Cr monolayers or sub-monolayers on Fe(001) has been investigated by a number of groups with different experimental techniques [85–97]. However, there is considerable disagreement between the corresponding experimental investigations and also between the experimental and the theoretical results. For example, Jungblut *et al* [85] used spin resolved core-level photoemission spectroscopy (SPPS) and estimated the Cr moment to be about 1 μ_B for a ferromagnetic Cr monolayer coupled antiferromagnetically to Fe(001). From a similar SPPS study by the same group a value of 0.5–1.0 μ_B/atom is reported [86]. A spin polarized electron-energy loss spectroscopy (SPEELS) study by Walker *et al* [87] measured

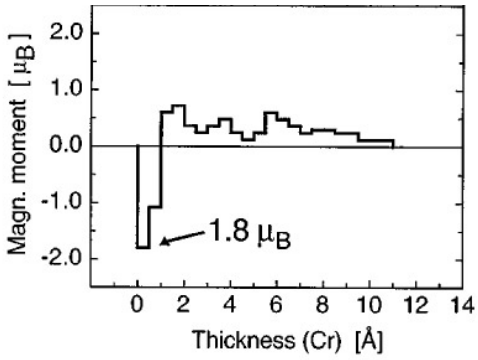

Figure 18. Magnetization profile of a thin Cr overlayer on Fe(001) obtained from energy resolved and spin polarized secondary-electron emission (from Fuchs *et al* [90]).

the exchange asymmetry of Cr monolayers on Fe and found that it has the opposite sign to the Fe spectrum and an enhanced magnetic moment. From an exchange splitting of 1.9 eV they infer a moment of roughly 1.9 μ_B/atom for 1 ML Cr on Fe. Furthermore, with increasing coverage the exchange asymmetry oscillates with a period of 2 ML, clearly indicating the antiferromagnetic order of Cr within this thickness range. Idzerda *et al* [88, 89] deduced the magnitude of the magnetic moment from soft-x-ray magnetic circular dichroism measurements and found 0.6 μ_B for a Cr coverage equal to 0.25. In contrast, Fuchs *et al* [90] find by energy resolved spin polarized secondary-electron emission a large spin polarization of Cr on Fe with a magnetic moment of 1.8 ± 0.2 μ_B/atom coupled antiparallel to Fe. The polarization changes sign after completion of the first monolayer and remains positive for thicker layers. These results, reproduced in figure 18, are in general agreement with SPPS experiments by Xu *et al* [91], reporting also a magnetic moment of 1.8 μ_B/atom for a submonolayer coverage. Finally, a recent and controversial study by Turtur and Bayreuther [92], using an *in situ* alternating gradient magnetometry technique, determined a magnetic moment of about 4 μ_B/atom antiparallel aligned for the first Cr monolayer on Fe.

Several authors have tried to explain the disagreements among the experimental results. From an experimental point of view, the Cr magnetism is highly sensitive to the structure of the interfaces and to interfacial roughness as suggested by the study of Cr on Fe(001) whiskers by Davies *et al* [78]. Surface preparation and cleanness is therefore of utmost importance.

Only a few reports have been published on the surface magnetism of bulk Cr, probably due to the difficulties encountered in preparing a clean surface. During repeated cleaning cycles residual contaminations diffuse to the surface and may change the surface structure and magnetism. Klebanoff has studied the Cr surface by angle resolved photoelectron spectroscopy [93–95]. The spectral features are claimed to be consistent with a surface-sensitive enhancement of the 3d polarization, yielding evidence that the Cr(001) surface is in a ferromagnetic state with an associated surface magnetic moment of 2.4 μ_B/atom. From the temperature dependence of the splitting of the surface resonance state a transition temperature of 780 K was estimated.

Berger and Hopster [96] have studied indirectly the Cr(001) surface by depositing Fe films with different thicknesses and measuring magnetic hysteresis loops of the top layer via the magneto-optical Kerr effect. The coercivity field showed a strong temperature dependence below 130 K, independent of the Fe film thickness, resembling a phase transition. Clearly this effect is connected with the Fe–Cr antiferromagnetic interface exchange coupling and possibly reflects the bulk spin flip transition, which occurs at $T_{SF} = 123$ K. Similarly the

interface exchange coupling of thin Fe on stepped Cr(001) with steps parallel to the [100] direction was investigated by Escorcia-Aparicio *et al* [97]. Above the bulk Néel temperature the steps induce a uniaxial magnetic anisotropy with easy axis parallel to the step edges along the [100] direction, whereas for $T < T_N$ the interface coupling favours the Fe magnetization perpendicular to the step edges if the step density is low.

Wiesendanger *et al* [98] performed STM measurements on the Cr(001) single crystal surface. Using a ferromagnetic CrO_2 tip and spin polarized tunnelling techniques they observe a periodic alteration of the step height between larger and smaller values compared to the non-polarized detection of the step height, which the authors interpret as being due to a topological antiferromagnetism as proposed by Blügel *et al* [26].

In conclusion, the surface studies agree on the fact that 1 ML of Cr on Fe is ferromagnetically ordered, exhibits an enhanced magnetic moment and is oppositely polarized to the Fe substrate. The exact value of the surface moment is converging to about 1.9 μ_B, which is a factor of two lower than theoretical predictions. This may still be the result of unavoidable intermixing at the Cr/Fe interface.

5.3. Spin density waves in Cr films

5.3.1. Cr films interacting with paramagnetic boundary layers. The spin density wave magnetism in thin epitaxial Cr films has recently been investigated via x-ray and neutron scattering by Sonntag *et al* [59, 99]. Cr(001) films were grown on an $A_2O_3(1\bar{1}02)$ substrate with an Nb(001) buffer layer. Aside from a native oxide layer, these films were not covered by another metallic film. The most prominent features of the SDW in thin epitaxial Cr films comprise a single $\vec{Q}_\pm$-state propagating perpendicular to the growth plane, a period for the I-SDW which is much larger than in bulk and which scales with the inverse film thickness and a spin flip transition from longitudinal to transverse I-SDW shifting up in temperature as the film thickness decreases. The single and longitudinal $\vec{Q}_\pm$-state oriented perpendicular to the plane becomes more prominent with decreasing film thickness. Figure 19 reproduces the SW satellite reflections close to the (002) Bragg reflection in a 3000 Å thick Cr(001) film for different temperatures as revealed by scattering experiments with synchrotron radiation. The (002) Bragg reflection is taken out for clarity. The temperature dependent $\vec{Q}_\pm$-position and intensity approaching the Néel transition is clearly visible. Additional neutron scattering shows that above the Néel temperature a fraction of the sample remains in a C-SDW persisting up to about 400 to 500 K. One of the samples used for scattering experiments (2500 Å thick Cr(001) film on a 500 Å thick Nb buffer layer) was also examined with PACS methods by Meersschaut *et al* [63] in order to test the comparability of these two techniques for determining SDW order in thin films. The PACS experiments confirm that the spins are oriented out of plane and that the I-SDW has longitudinal character with no flip transition up to the Néel temperature of 325 K. Above this temperature the sample is in a paramagnetic state with a small fraction of the sample (15%) still being in a commensurate state. In the commensurate state the hyperfine field is substantially enhanced, reflecting a Cr magnetic moment of 0.9 μ_B.

The Nb substrate provides an in-plane tensile stress on the Cr film. In bulk samples, $\vec{Q}_\pm$ would then be oriented parallel to the tensile stress axis, which is in conflict with the observations for Cr films on Nb. It appears that the electronic boundary condition between Cr and Nb plays a more important role than the stress for the orientation of $\vec{Q}_\pm$. On the other hand, the SDW period and the spin flip transition, which scale with the film thickness are indicators for the residual stress in the Cr film.

Bödeker *et al* [48, 56] have also determined the effect of a 20 Å thick Cu cap layer on the phase diagram of 2000 Å Cr(001) film via neutron scattering. They found that the cap

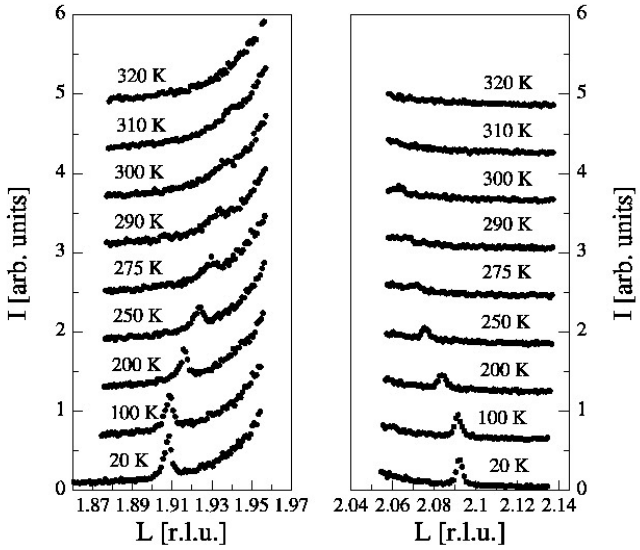

Figure 19. Strain wave satellite reflections on both sides of the Cr(002) reflection of a 3000 Å thick Cr(001) film on Nb/sapphire over a temperature range from 20 to 320 K, measured with synchrotron radiation (from Sonntag *et al* [59]).

layer has no effect on the longitudinal character of the I-SDW, again existing from the lowest temperature up to the Néel temperature. As in the uncovered Cr film, the spin flip transition is suppressed. A commensurate SDW becomes noticeable close to the Néel temperature, in agreement with the uncovered Cr film. Bödeker *et al* noticed that the Pd cap layer improves the coherence length of the SDW order in the Cr film as compared to those interacting with ferromagnetic cap layers. This may be caused by an exchange enhancement via the Pd cap without introducing frustration effects at interfaces containing steps. In figure 20 scattering results from the same Pd/Cr heterostructure using synchrotron radiation are shown. In contrast, a Cu cap layer is essentially inert, and the SDW order and phase transition is comparable to that of an uncovered Cr film [56].

Recently the SDW magnetism in Ag/Cr(001) superlattices was probed with PAC methods by Demuynck *et al* [62]. Ag/Cr superlattices are promising as model systems for studying the intrinsic SDW magnetism of Cr in confined environments without interference with proximity effects. The Cr spacer thickness was varied from 30 to 80 Å, just above the critical thickness for the stability of a I-SDW. In spite of the rather good lattice match a strong out-of-plane contraction of the Cr lattice parameter is observed in the superlattice. The PAC time spectrum uniquely determines that an I-SDW with spins normal to the plane exists. From the hyperfine field it is inferred indirectly that the I-SDW has longitudinal character. Contrary to the neutron results for Cr on Nb, the longitudinal SDW (AF_2) phase in Ag/Cr multilayers exists from the lowest temperature up to 500 K, where it suddenly disappears. Demuynck *et al* argue that the enhanced stability of the AF_2 phase is due to the structural properties of the sample, in particular due to the tetragonal distortion of the Cr layer. Decreasing the Cr spacer thickness from 59 to 51 Å leads to a complete collapse of the I-SDW with no indication for the existence of a C-SDW order. For this thickness the hyperfine field is quenched indicative for a paramagnetic state of the Cr film.

Mibu and Shinjo [65, 66] investigated Sn/Cr multilayers via Mössbauer hyperfine fields at the ^{119}Sn nuclear sites in the Sn layer. Multilayers with different Sn thicknesses but fixed Cr

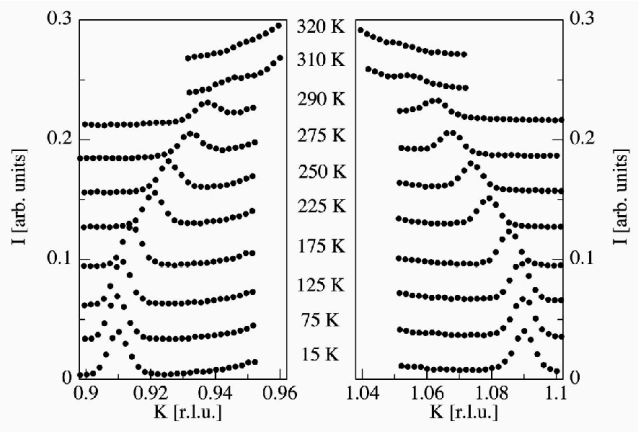

Figure 20. Measurements with synchrotron radiation probing the strain waves in a 2200 Å thick Cr(001) film capped with a 20 Å thick Pd layer. The scans, taken for different temperatures and along the K direction across the (110) reflection, reveal an in-plane orientation of $2\vec{Q}_{\pm}$. Corresponding neutron scattering measurements confirm that the SDW in Pd/Cr heterostructures has a partial transverse polarization with $\vec{Q}_{\pm}$ in the film plane and partial longitudinal polarization with $\vec{Q}_{\pm}$ out of plane (from Bödeker *et al* [56]).

thickness of 50 Å show a large distribution of hyperfine fields at room temperature, indicating Cr spin order. The maximum hyperfine field observed is larger than for Sn dissolved in Cr, and even larger than for Sn in Fe or Co matrix. Mibu *et al* interpret this result as due to the contact of Sn with the Cr layer and the penetration of spin polarized electrons into the Sn layer. Vice versa, if for a constant Sn thickness of 20 Å the Cr layer thickness is varied between 30 and 100 Å, the hyperfine field at 300 K stays roughly the same, indicating that Cr is in a magnetically ordered state over the whole thickness range. Even in Cr/Sn epitaxial multilayers with a Cr layer thickness between 2 and 40 Å very large hyperfine fields were found, characteristic for their antiferromagnetic order at room temperature and possible enhanced Néel temperature. A distinction between C- and I-SDW is not possible with this method.

The experimental situation for Cr films in contact with paramagnetic layers is not clear at the present time. Besides the compatibility check on one of the samples, there exists an uncomfortable disagreement between some of the neutron and PAC data. Both techniques agree that in Cr films, which are in contact with paramagnetic boundary layers, the L-SDW (AF_2) phase is predominant and that the spin flip transition is suppressed. Tetragonal strains are considered to be responsible for this. However, for all samples the tensile strain is in the plane, and therefore an in-plane orientation of the SDW wave vector would have been expected. Furthermore, strain also induces a C-SDW, but a commensurate phase is either not observed at all (Cr/Ag) or remains a minority phase (Cr/Nb and Cr/Nb/Cu). The high Néel temperature for the incommensurate phase in Cr/Ag is totally unexpected, in particular since proximity effects are not at work to support this spin structure. In Cr/Sn the presumable C-SDW order appears enhanced whereas in Ag/Cr a collapse of the C-SDW order is observed. Whether an antinode exists at the Cr/noble metal interface, as expected for smooth interfaces, is not known.

5.3.2. Thin Cr films in contact with ferromagnetic layers. First we shall briefly describe the by now classical experiments by Unguris *et al* [100, 101]. This group has deposited a Cr wedge on an Fe whisker with (001) orientation and covered the wedge with a thin Fe film. The domain structure of the top Fe layer was imaged by a scanning electron microscope with

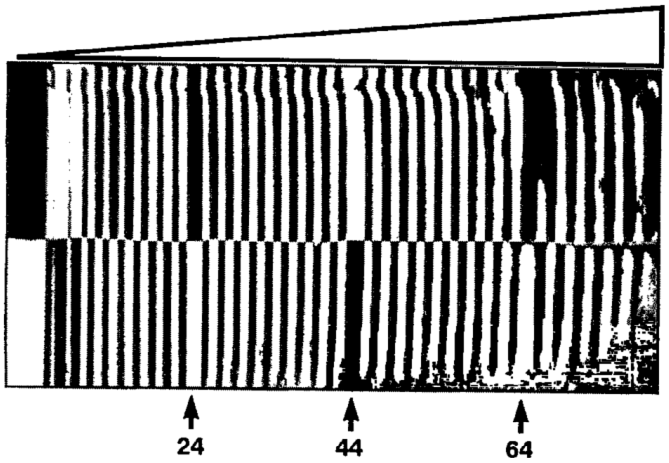

Figure 21. Image of the domain structure in an Fe layer covering a Cr(001) wedge grown on an Fe(001) single crystal whisker substrate. The image was taken with a scanning electron microscope including polarization analysis of the secondary electrons (SEMPA). The arrows mark Cr layer thickness in monolayers where phase slips in the domain structure occur, due to the incommensurability of the SDW (from Unguris *et al* [100]).

polarization analysis (SEMPA). Figure 21 reproduces the SEMPA results. Dark and white stripes alternate, whenever the Cr thickness changes by one ML. Two sets of striped domains run parallel along the whisker axis shifted by a constant phase factor π, because the whisker contains two antiparallel Fe domains with the magnetization vectors oriented along the whisker axis. The striking feature of these experiments can be summarized as follows. The domains alternate in the lateral direction with a periodicity of two Cr monolayers. Periodic phase slips are visible at positions 24, 44 and 64, i.e. at distances of 20 ML. At the phase slips, even and odd numbers of Cr MLs lead to the same coupling. For $N < 23$, F coupling occurs for an even N rather than for an odd N, as would have been expected for an ideal interface. This has been attributed to interfacial roughness and alloying of the first Cr ML on the Fe whisker, as observed by Pierce *et al* [80] and Davies *et al* [78]. For $N < 23$, the Cr spacer appears to be C-SDW ordered. The first node indicates I-SDW order for $N > 23$. The incommensurate order is stable at least up to 550 K, beyond which interdiffusion takes place and destroys the heterostructure. The distance between the nodes depends on the temperature and increases smoothly up to 550 K, similar to the increase of $\vec{Q}_{\pm}$ with temperature observed in bulk Cr (figure 22). In contrast to bulk properties, in the Cr wedge I-SDW order exists far above the bulk Néel temperature, at least up to 1.8 T_N, and for a Cr thickness of at least 70 ML.

These beautiful experiments tell us many features about SDW magnetism in thin Cr films without really seeing the spin structure. In spite of the interface roughness, the Fe–Cr interface coupling is still strong enough to place an antinode at the interface and induce proximity magnetism in the Cr layer which withstands temperatures as high as 1.8 T_N. Whenever the Cr thickness is incremented by one monolayer, the Fe in-plane magnetization switches direction. Thus magnetic domains are not created in the Cr film but in the top Fe layer to overcome possible frustration effects following a step at the Fe–Cr interface. Stretching of the SDW as predicted by Shi and Fishman [36] seems not to take place since the distance between phase slips is constant and in fact lower than in the bulk at the same temperature. The highly regular pattern points to a rather rigid SDW period. The distance between the steps is larger than the average magnetic domain wall thickness in the Fe layer. Therefore the magnetic domains in

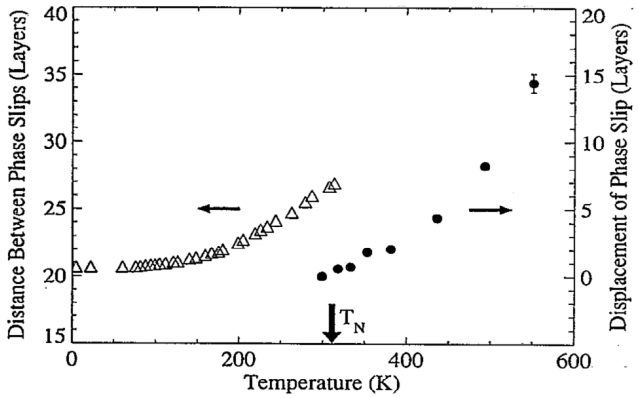

Figure 22. The temperature dependence of the distance between nodes of the SDW ($1/\delta$) for bulk Cr according to [11] (open triangles) and for the Fe/Cr/Fe heterostructure shown in figure 21 as determined by the distance between the phase slips (solid circles). The arrow marks the bulk Néel temperature. The SDW in the Cr wedge exists to much higher temperature than in the bulk (from Unguris *et al* [100]).

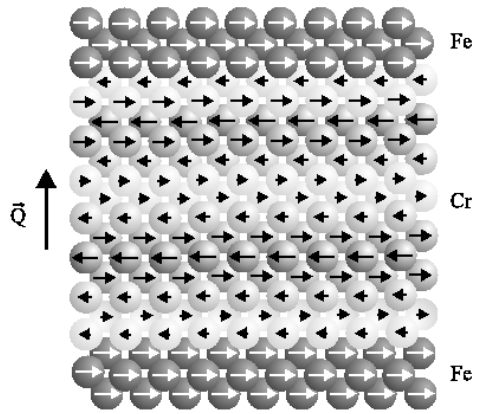

Figure 23. Schematic representation of the ideal magnetic structure depicted for the situation present in 250 Å thick films in proximity with Fe layers. The incommensurate spin-density wave propagates in the out-of-plane direction and the Cr spins are oriented in the plane, allowing for an antiferromagnetic exchange interaction at the Fe/Cr interface.

the top Fe layer can follow the directional change of the Cr spins at the Fe–Cr interface. This is another proof of the fact that the surface of Cr is ferromagnetically ordered with a layered antiferromagnetic structure. From these visual inspections we can infer that in the Cr film the I-SDW is transverse with $\vec{Q}_{\pm}$ perpendicular to the plane and spins in the plane, as sketched in figure 23.

The SDW order in Fe/Cr multilayers was also investigated by Fullerton *et al* with neutron scattering [102]. For a Cr thickness of 115 Å the structure factor around the (001) reflection exhibits two satellite reflections at positions comparable to those in the bulk. From the position of the satellite reflections and using the selection rules for neutron scattering, it can be inferred that in the Fe/Cr multilayer a transverse I-SDW exists with $\vec{Q}_{\pm}$ normal to the layers. The neutron scattering data are shown in figure 24. No evidence for a longitudinal SDW has been seen nor

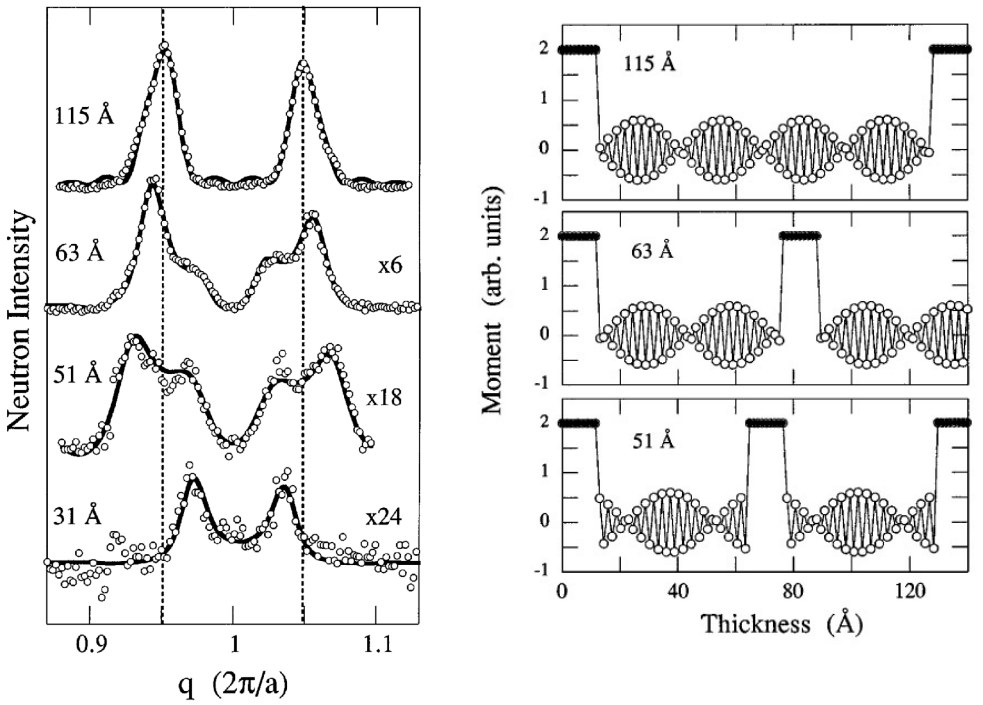

Figure 24. Neutron scattering from Fe/Cr superlattices with different Cr spacer thickness. The left panel shows the experimental neutron scattering results; the right panel reproduces the results of a structure factor analysis for the determination of the magnetization profile in the Cr layers (from Fullerton *et al* [102]).

for an SDW with an in-plane $\vec{Q}_{\pm}$, asserting that the Cr layers are in a single $\vec{Q}_{\pm}$-state. For thinner Cr layers the scattering pattern becomes more complex. A careful structure factor analysis shows that the SDW period is independent of the thickness. However the phase changes with thickness. As figure 25 shows, for multilayers with a Cr thickness of 115 and 63 Å the nodes of the SDW are located close to the interface. For 51 Å thick Cr the antinode lies at the Fe–Cr interface and two nodes occur in between, forming half an SDW period. Below this thickness the SDW order collapses, and for 31 Å Cr possible C-SDW order may exist. The temperature variation of the structure factor shows that the Néel temperature depends on the Cr layer thickness, in good agreement with magnetic hysteresis measurements by the same authors, indicating finite size scaling of the bulk Néel temperature with decreasing Cr film thickness [103].

Schreyer *et al* [104] have studied with neutron scattering an Fe/Cr(001) superlattice with a Cr thickness of 80 Å and compared interlayer exchange coupling with SDW order. While at low temperatures a transverse I-SDW exists with $\vec{Q}_{\pm}$ normal to the film, I-SDW order vanishes by passing a transition region above $T_N(t_{Cr} = 80\ \text{Å}) = 200$ K and is replaced by a C-SDW. The C-SDW exhibits a much higher Néel temperature T_{NC} of about 500 K. The same sample was also examined by reflectivity experiments with polarized neutrons probing the Fe-layer magnetization vectors [105]. Combining both scattering techniques it was concluded that in the low temperature I-SDW phase the exchange coupling is weak, whereas in the high temperature C-SDW phase the Cr spin structure mediates a strong exchange coupling, causing the magnetization vectors of adjacent Fe layers to enclose a non-collinear angle. This notion has been confirmed by several neutron

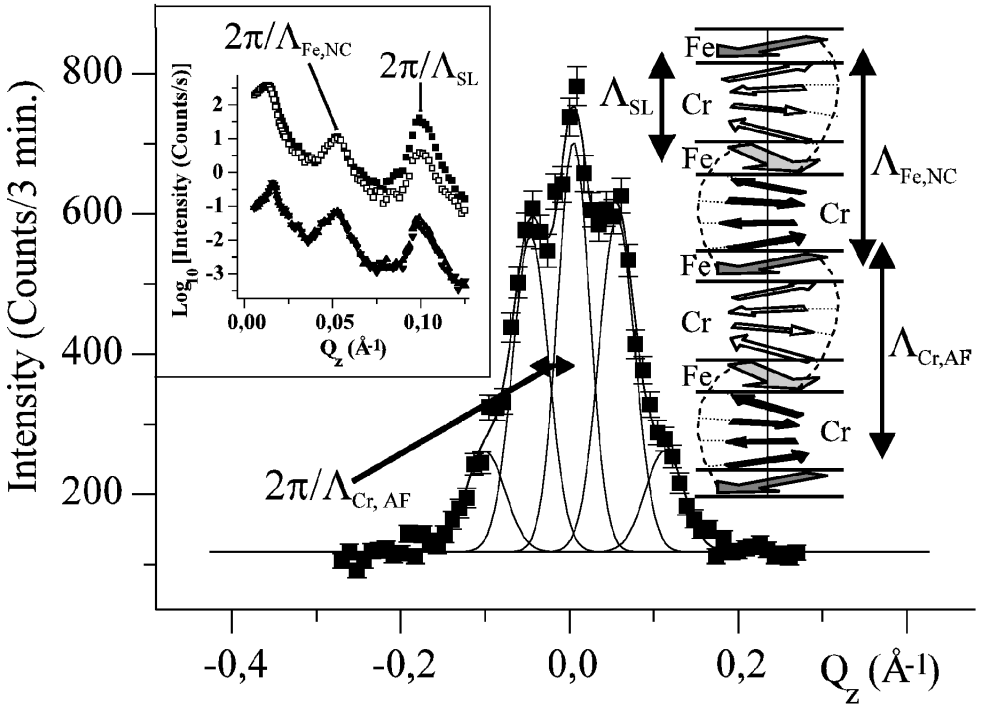

Figure 25. Neutron scattering from an Fe/Cr superlattice with a Cr spacer thickness of 42 Å. In the centre is shown a scan at the (010) Bragg position in the z-direction. The commensurate Cr(010) peak is modulated by the magnetic superlattice periodicity, which has twice the chemical periodicity. The inset in the upper left corner shows polarized neutron reflectivity data, revealing a non-collinear arrangement of the Fe layer magnetization vectors. In the upper right inset is sketched the most reasonable spin structure in the Fe/Cr superlattice with respect to the experimentally determined boundary conditions. Those include a non-collinear Fe magnetization, a doubling of the magnetic periodicity compared to the chemical and a commensurate Cr spin structure, which is twisted in order to take advantage of the interface exchange coupling (from Schreyer *et al* [104]).

scattering experiments on Fe/Cr(001) superlattices [104–109]. In particular, for an Fe/Cr superlattice with a Cr spacer thickness of 40 Å, neutron scattering studies confirmed a non-collinear Fe layer magnetization together with a commensurate Cr spin structure being modulated by the same periodicity as the Fe layers. The neutron scattering results are reproduced in figure 26 from the work of Schreyer *et al* [104]. They are consistent with the proximity magnetism model discussed in section 3.4 for an intermediate level of interface roughness.

Neutron diffraction and reflectivity studies by Fullerton *et al* [102, 106] and Adenwalla *et al* [107] on Fe/Cr(001) superlattices grown on MgO(001) substrates confirm these results. These authors believe, however, that in thin Cr layers the interface disorder may be sufficiently high to suppress either the long range order of the Cr moments or the magnitude of their magnetic moments, such that Cr would exhibit only local order or be in a paramagnetic state. In contrast, the neutron scattering results by Schreyer *et al* [104, 108] assure that whenever Cr is not in an I-SDW state, it is commensurate antiferromagnetic due to the proximity with the ferromagnetic Fe layers, more precisely in a helical state. These conflicting statements about the Cr spin order in very thin films are most likely due to different levels of interface roughness, which, in turn, depends on the growth methods and substrates chosen.

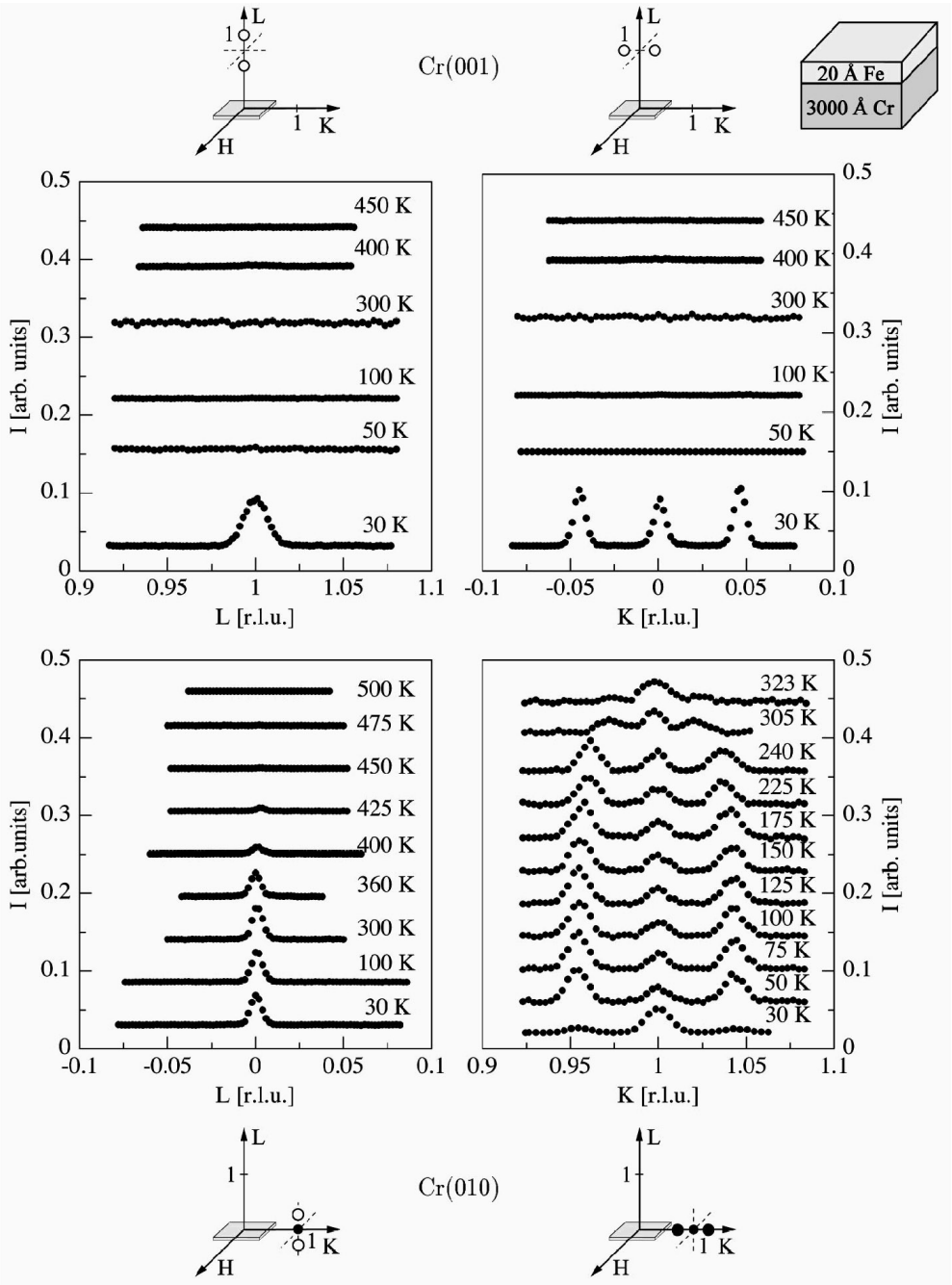

Figure 26. Neutron scattering on a 3000 Å thick Cr(001) film covered with a 20 Å thick Fe(001) layer to explore the orientation and polarization of the spin-density waves for different temperatures from 30 to 450 K. Scans are shown in different directions in the reciprocal space as sketched close to the respective panels, where the filled circles represent existing peaks while open circles indicate satellite positions scanned but no intensity detected at 50 K (from Bödeker *et al* [56]).

Meersschaut *et al* [60] have studied the SDW order in an Fe/Cr(001) superlattice by the PAC method and found for a Cr thickness between 40 and 60 Å an I-SDW phase at low temperatures and a rapidly increasing Néel temperature with increasing film thickness. For a Cr thickness between 75 and 400 Å this group determined from the PAC time spectra a longitudinal SDW structure with spins and $\vec{Q}_{\pm}$ oriented normal to the plane. The Néel temperature for this spin structure was reported to be much higher than in bulk Cr. For a thickness below 60 Å, no magnetic moment of Cr could be detected and it was concluded that Cr would be non-magnetic or paramagnetic below 60 Å.

Although the exchange coupling and in particular the biquadratic coupling, as we noted, is strong only for a commensurate Cr spin structure, it is still much weaker than expected theoretically. Recent studies by Venus and Heinrich [79] show that the interface exchange coupling at the Fe/Cr interface is 1/30 smaller than expected for perfect coupling without interface roughness, as determined by first principles calculations (Stoeffler and Gautier [110]).

5.3.3. Thick Cr films in contact with ferromagnetic layers. After discussing the thin film case, we now turn our attention to thicker Cr films in contact with ferromagnetic boundary layers. Bödeker *et al* [48, 56] have studied the SDW order in Cr(001) films in contact with ferromagnetic layers via x-ray and neutron scattering. Starting with a Cr film thickness of 3000 Å covered with a 20 Å thick Fe layer, a single $\vec{Q}_{\pm}$ state and transverse I-SDW is expected below T_N with $\vec{Q}_{\pm}$ oriented perpendicular to the film plane because of the in-plane magnetization of the Fe layer and the AF coupling at the Fe–Cr interface, as sketched in figure 23. Contrary to expectations, the scattering experiments univocally show that $\vec{Q}_{\pm}$ is oriented parallel to the film plane with the Cr magnetic moments pointing in the direction normal to the film plane and to the Fe in-plane magnetization. A typical neutron scattering experiment from a 3000 Å thick Cr(001) film capped with a 20 Å thick Fe(001) layer is shown in figure 26. The scans are taken at four specific points in reciprocal lattice to ascertain the orientation and polarization of the I-SDW.

The transverse I-SDW with in-plane orientation of $\vec{Q}_{\pm}$ has been explained by Bödeker *et al* [48] and Hucht [49] in terms of steps and kinks at the interface, as discussed in section 3.4. A transverse I-SDW with in-plane orientation of $\vec{Q}_{\pm}$ and spins out of plane has also been reported for about 3000 Å thick Cr films covered with Ni or Co cap layers. In none of the cases do the cap layers change the Néel temperature, remaining bulk-like for this thickness range [56].

Upon reduction of the Cr film thickness, Bödeker *et al* [56] observe a rotation of $\vec{Q}_{\pm}$ from in-to out-of-plane orientation. The re-orientation starts at a Cr thickness of about 750 Å and is completed at about 250 Å. Neutron scattering results from a 250 Å thick Cr film sandwiched between Fe layers are shown in figure 27. The reorientation of the SDW is obvious by comparing figures 26 and 27. Bödeker *et al* argue that below 250 Å interfacial exchange coupling wins over the frustration effects, the Cr layer thickness for which the transition occurs being an indication of the average terrace length. A qualitative phase diagram for the orientation of the spin-density waves in epitaxial Cr(001) films covered with a thin Fe layer as a function of the Cr film thickness is reproduced in figure 28 from the work of Bödeker *et al* [56]. It reproduces the situation present at about 100 K.

5.3.4. Scaling of the Néel temperature. The earliest report of a thickness dependence of the Néel temperature was given by Mattson *et al* [73]. By measuring the resistivity they observed a reduction of T_N from the bulk value at 3000 Å to 235 K at 400 Å. The authors concluded that the reduction is due to epitaxial stress from the lattice mismatch between the Cr film and the LiF substrate, which becomes enhanced due to a mismatch of the thermal expansion

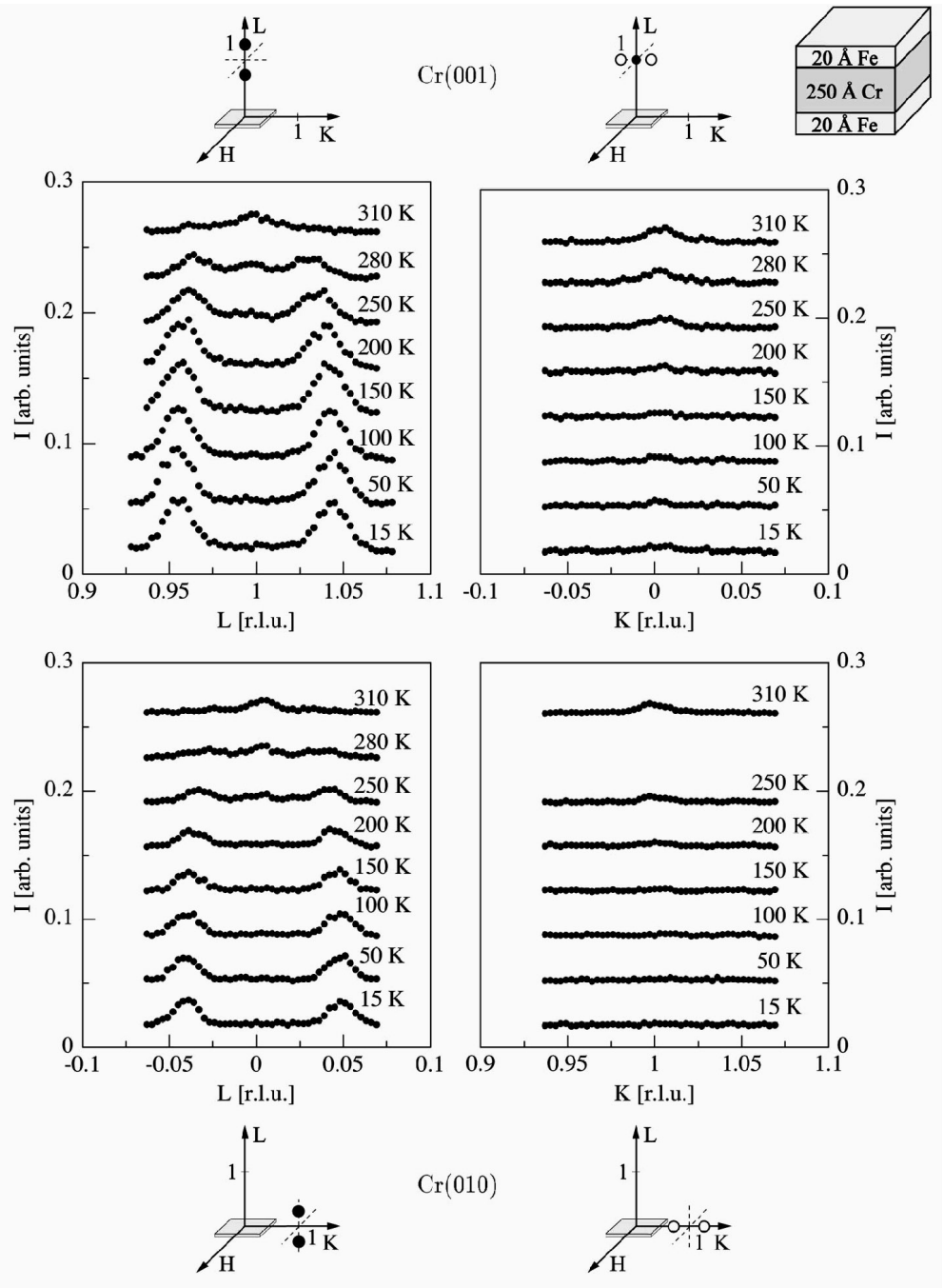

Figure 27. Neutron scattering results probing the spin density wave in a 250 Å thick Cr film sandwiched between 20 Å thick Fe layers all with (001) orientation. From the observation of satellite reflections at the positions $(0, 0, \pm\delta)$, $(0, 1, \pm\delta)$ it can be inferred that the spin density wave is transverse with $\vec{Q}_{\pm}$ oriented parallel to [001] (from Bödeker *et al* [56]).

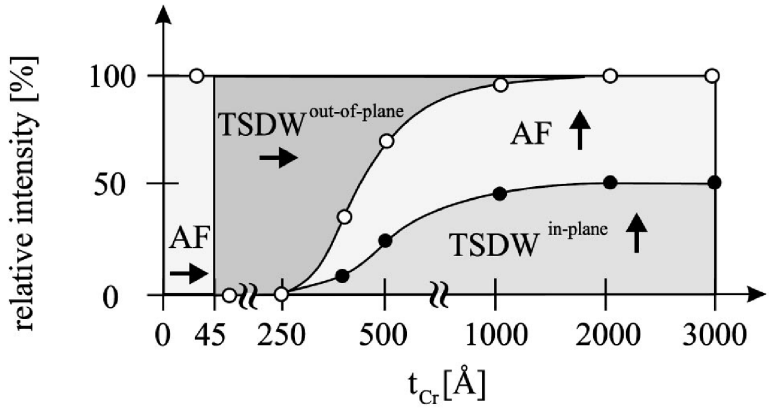

Figure 28. Qualitative phase diagram of the spin-density waves in epitaxial Cr(001) films covered with a thin Fe layer as a function of the Cr film thickness. The phase diagram represents the situation at about 100 K. The arrows indicate the orientation of the Cr magnetic moment, where the vertical direction corresponds to spins oriented perpendicular to the film plane (from Bödeker *et al* [56]).

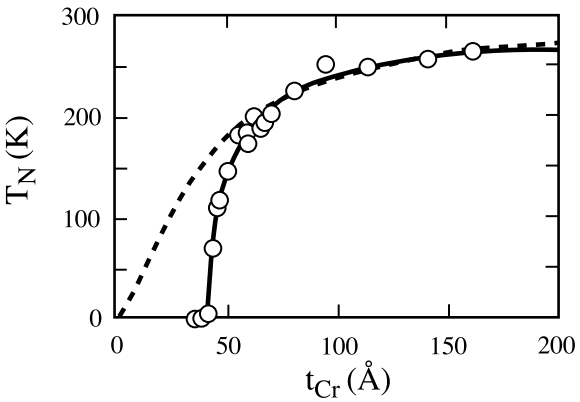

Figure 29. The Néel tempeature T_N for a series of [Fe(14 Å)/Cr(t_{Cr} Å)]×13 superlattices against Cr thickness t_{Cr}. The open circles are the measured values, and the dashed and solid curves are fitted by equations (8) and (15), respectively (from Fullerton *et al* [103]).

coefficients at low temperatures. It is well established that the Néel temperature exhibits a negative uniaxial pressure coefficient thus explaining rather well the shift of T_N with Cr film thickness. A possible scaling effect could not be separated.

Fullerton *et al* [103] have shown via transport measurements and magnetic hysteresis curves that the biquadratic coupling of Cr observed for $T > T_N$ becomes reduced below T_N, the Néel temperature depending critically on the Cr film thickness in Fe/Cr/Fe trilayers. The scaling of the Néel temperature with the layer thickness is expected to follow equation (8). However, the experiments show a strong deviation from the simple scaling behaviour at low temperatures, pointing to the existence of a magnetically dead layer with thickness t_0. Rephrasing equation (8) yields

$$\frac{T_N(\infty) - T_N(t_{Cr})}{T_N(t_{Cr})} = b(t_{Cr} - t_0)^{-\lambda'} \tag{14}$$

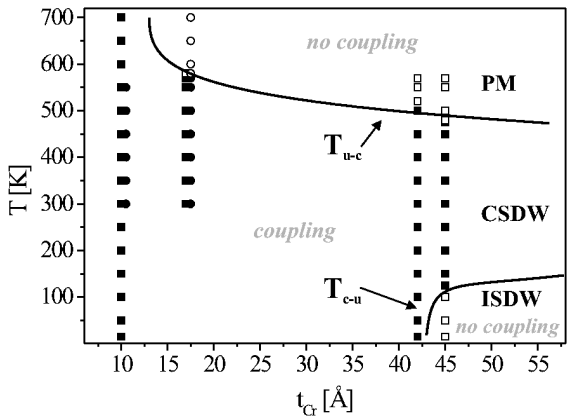

Figure 30. Magnetic phase diagram of the Fe/Cr system as determined by magneto-optical Kerr effect and neutron scattering experiments. The solid lines separate regions for the incommensurate, commensurate and paramagnetic state of Cr as a function of Cr layer thickness and temperature. The solid line between the CSDW and ISDW states exhibits the scaling behaviour already visible in figure 29. The solid line between the CSDW and PM phases is due to the proximity induced antiferromagnetic order in Cr via the Fe layers. The different regions can also be characterized by their exchange coupling strength between the Fe layers. T_{u-c} and T_{c-u} then designate the transition temperatures between uncoupled and coupled Fe layers, and vice versa, respectively (from Schmitte *et al* [111]).

which fits much better the experimental results, as shown in figure 29. Below a thickness of $t_0 =$ 44 Å or 30 ML the Néel temperature for the I-SDW completely vanishes. Thus the hysteresis measurements yielded two important results about the SDW magnetism in thin Cr films: scaling behaviour of the Néel temperature and a collapse of the I-SDW magnetism for film thicknesses smaller than 30 ML. This critical thickness matches about the extension of half a period of the I-SDW in Cr at low temperatures. In contrast, the experiments by Unguris *et al* [100] clearly show AF order starting with the first Cr monolayers. The contradiction is lifted by considering the interface quality. As discussed previously, a smooth interface allows a maximum coupling of the Cr spins to the Fe layers, including a proximity enhanced magnetism even above T_N and below a Cr thickness for which an I-SDW would not be possible. However, for a rough interface a node is required at the interface excluding C-SDW order. Then the limit for I-SDW order corresponds to half a SDW period or about 30 ML, in very good agreement with the results by Fullerton *et al* [102] and Schreyer *et al* [104]. In figure 30 a combined phase diagram including neutron scattering results of Schreyer *et al* [104] and magneto-optical Kerr effect measurements of Schmitte *et al* [111] is reproduced. The solid line between the I-SDW and C-SDW is in agreement with the results of Fullerton *et al* [102]. According to this phase diagram the Néel temperature for the I-SDW scales with the film thickness, similar to the phase diagram shown in figure 29. In addition it shows that outside of the existence region of the I-SDW, Cr exhibits either a commensurate, helical or mixed spin structure. In particular, for a thickness below 30–40 Å, Cr is in a commensurate state. The commensurate antiferromagnetic structure exhibits a higher Néel temperature of roughly 500 K, which increases slightly with decreasing film thickness.

Using FMR spectroscopy from a capping Fe layer deposited on Cr films, Pflaum *et al* [112] observed a strong temperature dependence of the resonance field. At a characteristic temperature the resonance field deviates from a linear behaviour. Identifying this temperature as the spin flip transition, Pflaum *et al* find a scaling behaviour of the spin flip temperature with Cr thickness for a thickness range of 30 Å $< t_{Cr} <$ 5000 Å. A similar observation was

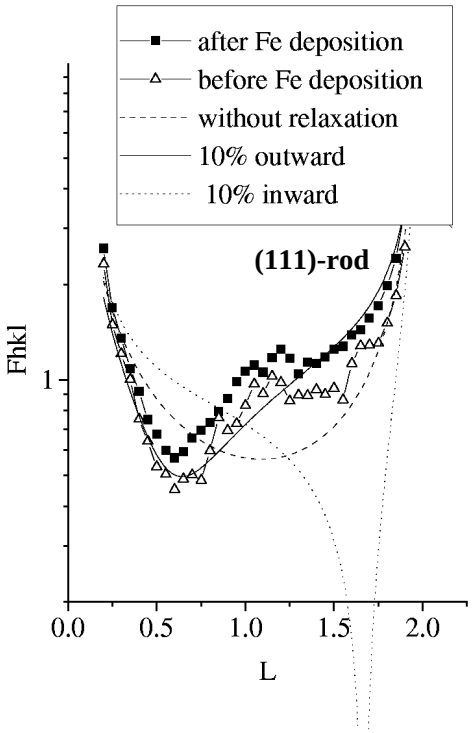

Figure 31. (11L) crystal truncation rod measurements of the plain Cr(001) surface and after deposition of three monolayers of Fe. The hump between the (110) and (111) reflection is due to a relaxation of the top surface layer. Model calculations show it can only be described by the assumption of an outward relaxation of about 10% (from Stierle *et al* [113]).

made by Pflaum *et al* for the coercivity of the Fe film, which also scales with the Cr film thickness. If both scaling behaviours are identified with the spin flip transition between the AF_1 and AF_2 phase, then a completed suppression of the spin flip transition is observed below a Cr film thickness of 60 Å. This cut-off is similar to the one discussed above for the scaling of the I-SDW. The mechanisms for the spin flip transition in thin exchange coupled Cr films with fixed boundary conditions to the Fe layers is, however, not clear.

5.3.5. In situ studies of Cr spin density waves. Cr films in contact with paramagnetic layers or with vacuum exhibit an L-SDW with $\vec{Q}_{\pm}$ perpendicular to the film plane. Neutron scattering and PAC experiments agree on this fact, although the reason for it is not yet clear. As soon as the Cr film is in contact with a ferromagnetic layer the boundary conditions are changed and interface structure and exchange dictates the orientation and polarization of the SDW. It would be interesting to investigate the change of the boundary condition *in situ* during deposition of ferromagnetic films on Cr. Stierle *et al* [113] have studied with synchrotron radiation the structure of a plain Cr(001) surface under UHV conditions and subsequently covered the Cr surface with several monolayers of Fe while successively studying structural changes as well as the satellite reflections from the strain wave. Figure 31 shows (11L) truncation rod measurements of the plain Cr surface. After several cleaning cycles the top Cr layer appears to be outward relaxed by 10%. This structural relaxation remains intact even after deposition of a few Fe monolayers. Scans along the $(H00)$, $(0K0)$, and $(00L)$ directions under surface

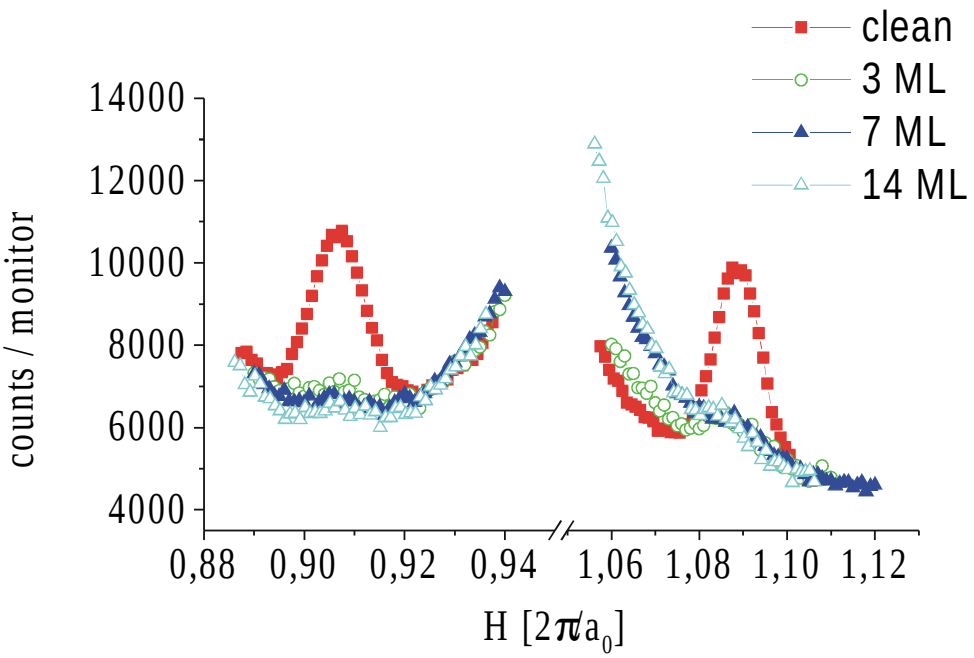

Figure 32. Surface sensitive synchrotron study of the strain waves in Cr(001). Scans are only shown for the in-plane [H00] direction. The clean Cr surface exhibits a strain wave parallel to the film plane, which vanishes almost completely after deposition of a few monolayers of Fe. The strain is then oriented along the [00L] direction and is associated with a transverse spin density wave (from Stierle *et al* [113]).

sensitive scattering conditions are sensitive to the strain waves close to the surface. An example is shown in figure 32. Before Fe deposition, SW satellite reflections are visible along the H and along the L direction (not shown here). After deposition of 3 ML of Fe the in-plane strain wave has almost completely vanished and only an out-of-plane strain remains. For a smooth Cr surface this is to be expected, since then only a transition from L-SDW to T-SDW takes place, both with $\vec{Q}_{\pm}$ normal to the film plane. On the other hand, for a rougher surface similar synchrotron experiments with *in situ* deposition of a few MLs of Fe show that a reorientation of the strain wave from perpendicular to parallel to the film indeed occurs, as expected from the spin frustration at the interface and in agreement with the experiments by Bödeker *et al* [48].

6. Summary and conclusions

The spin density wave magnetism in Cr films is as complex as it is spectacular and exquisite. The SDW is not a rigid property, but it depends on many factors such as temperature, film thickness, interface exchange coupling, hybridization with the adjacent layers and interface roughness. The principal mechanism of the SDW magnetism in thin Cr films can be understood on one hand by fulfilling the specific boundary condition at the interface and on the other hand by the intrinsic incommensurate SDW magnetism, favouring bulk values for the SDW amplitude and wave vector.

This review attempted to provide a brief overview of recent developments concerning the magnetism of Cr at the surface and in thin films. The main results can be stated as follows. The

surface magnetism of bulk Cr(001) clearly shows a ferromagnetic order with antiferromagnetic coupling to the subsurface layer. The surface magnetic moment may, however, be lower than expected theoretically. Stierle *et al* noticed an outward relaxation of the top surface layer, which may have an important impact on the magnetic moment density at the surface. Also the magnetic moment of a Cr monolayer on Fe(001) turns out to be lower than expected. Aside from the obvious reasons of interdiffusion and roughness at the interface, more fundamental reasons for this include a possible ferrimagnetic order of Cr as predicted theoretically and a reduction of the Fe moment in the subsurface layer.

Clear predictions exist for the spin structure of Cr monolayers on Pd, Pt and noble metals. However the experimental research is lacking behind those predictions, in part because of growth problems. The situation is better for Cr on Fe(001), for which a more consistent picture is emerging. Cr on Fe(001) exhibits a ferromagnetic order with a local moment of about 1.8 μ_B and is antiferromagnetically coupled to the Fe substrate.

The investigation of thin Cr films and the observation of SDW as they emerge with increasing thickness is most fascinating. Practically all theoretical and experimental studies have investigated {001} oriented Cr films, since this is the major axis for the orientation of the SDW. Cr in contact with vacuum or noble metals is predicted to exhibit an antinode at the interface, if the interface is smooth. On the other hand, at the interface between Cr and Mo and possibly also between other 4d and 5d metals, a node should exist. Experiments have not yet confirmed this. However, neutron scattering and perturbed angular correlation spectroscopy experiments agree that the longitudinal SDW is favoured over the transverse SDW if Cr is in contact with vacuum or with paramagnetic layers. There is some disagreement about the Néel temperature. While x-ray and neutron scattering results agree that the Néel temperature for the incommensurate SDW is never higher than in the bulk and eventually scales with the thickness, PAC experiments appear to indicate an enhanced Néel temperature in Cr/Ag superlattices.

Among the studies considering Cr/ferromagnetic interfaces, the Cr/Fe interface is the most important and intensively examined interface. Therefore we shall restrict our discussion to this interface. Furthermore, it is useful to distinguish between thick and thin layers and smooth or rough interfaces. For smooth interfaces and a Cr spacer thickness between Fe layers of less than 20 monolayers, Cr experiences a proximity enhanced magnetism with antinodes at the interface and a commensurate SDW in the spacer. If the Fe layers are free to rotate and adapt to the number of Cr monolayers in between, Cr remains antiferromagnetic down to the monolayer level and the Néel temperature of the commensurate phase increases with decreasing Cr thickness, proportional to the magnetic moment density of Cr. Beyond 20 monolayers a first node will appear, signalling the onset of intrinsic incommensurate SDW order. The SDW has transverse character with spins in the plane and orientation of the SDW perpendicular to the plane. Thus, the in-plane magnetization of the Fe layers and the antiferromagnetic exchange coupling at the interface between Fe and Cr single out one particular transverse SDW. The Néel temperature of the incommensurate SDW scales strongly with the Cr layer thickness. Furthermore, the period of the SDW is a function of temperature and expands with increasing temperature as in the bulk. Therefore, if for a finite film thickness an incommensurate SDW exists at low temperatures, a transition from an incommensurate to a commensurate phase occurs at higher temperatures, before the Cr films finally become paramagnetic at an even higher temperature.

If the interface is very rough, nodes are required at the interface and the Cr layer loses contact with the proximity enhancing neighbouring layers. Then the Cr layer has no choice but to be either in an incommensurate state for thick enough layers, or becoming paramagnetic with decreasing film thickness or increasing temperature.

The most interesting case is the one with an intermediate level of roughness. Point defects due to interdiffusion may be considered as gentle defects. They only shift the phase but leave the antinode close to the interface. Monatomic high steps constitute much more severe defects. If the step separation is smaller than the Cr film thickness, the orientation of the SDW ordering wave vector is being rotated from perpendicular to in plane, while preserving the transverse polarization. With decreasing film thickness the SDW resembles more the one for a smooth interface, trying to keep the antinode at the interface and setting up a transverse SDW with spin in the plane and wave vector out of plane. Upon further reduction of the film thickness an incommensurate–commensurate transition takes place similar to the situation for smooth interfaces. However, the steps at the interface are now compensated by two commensurate and twisted SDWs on either side of the step, turning counter-clockwise and coupling the Fe in-plane magnetization vectors in the top and lower layer at a non-collinear angle.

Although an almost consistent picture emerges from these studies of the spin density wave magnetism in thin Cr films, there is still a major discrepancy among the experimental data. Assuming almost perfect interfaces, the Néel temperature for the incommensurate–commensurate spin density wave scales with the thickness never exceeding the bulk value, as shown by the magnetic phase diagrams in figures 29 and 30, gained from neutron scattering experiments and magnetic hysteresis measurements. On the other hand, in a Cr film wedged between Fe layers the Néel temperature can be about twice as high as in the bulk, as shown in figure 22. Furthermore, since the distance between the nodes is a strong function of temperature, for a fixed number of Cr monolayers an incommensurate–incommensurate transition must occur in the Cr wedge with changing temperature, before reaching the phase boundary for the incommensurate–commensurate transition. This scenario is in accordance with theoretical predictions, but it has never been confirmed in Fe/Cr systems other than in the Fe-whisker/Cr-wedge/Fe film used by the NIST group. Thus the discrepancies pointed out may still be a question of interface quality.

Acknowledgments

I would like to thank P Bödeker, T Schmitte, A Schreyer, P Grünberg and D T Pierce for fruitful discussions. In particular I would like to thank A Stierle for permission to reproduce data prior to publication. This work has benefited from support by the Bundesministerium für Bildung und Forschung under contract 03-ZA4BC2-3, and the Landesministerium NRW für Wissenschaft und Forschung.

References

[1] Corliss L, Hastings J M and Weiss R J 1959 *Phys. Rev. Lett.* **3** 211
[2] Bykov V N, Golvikin V S, Ageev N V, Levdik V A and Vinogradov S L 1958 *Dokl. Akad. Nauk SSSR* **4** 1149
[3] Overhauser A W 1962 *Phys. Rev.* **128** 1437
[4] Bland J A C and Heinrich B 1994 *Ultrathin Magnetic Structures* vols I and II (Berlin: Springer)
[5] Fawcett E 1988 *Rev. Mod. Phys.* **60** 209
[6] Arrott A, Werner S A and Kendrick H 1967 *Phys. Rev.* **153** 624
[7] Teraoka Y and Kanamori J 1977 *Physica* B **86–88** 321
[8] Nakajama S and Kurihara Y 1975 *J. Phys. Soc. Japan* **38** 330
[9] Kotani A 1975 *J. Phys. Soc. Japan* **38** 974
[10] Hirai K 1993 *J. Phys. Soc. Japan* **62** 690
[11] Werner S A, Arrott A and Kendrick H 1962 *Phys. Rev.* **155** 528
[12] Gibbs D, Mohanty K M and Bohr J 1988 *Phys. Rev.* B **37** 562
[13] Hill J P, Helgesen G and Gibbs D 1995 *Phys. Rev.* B **51** 10 336
[14] Bastow T J and Street R 1966 *Phys. Rev.* **141** 510

[15] Fawcett E, Alberts L, Galkin V Y, Noakes D R and Yakhmi J V 1994 *Rev. Mod. Phys.* **66** 25
[16] Jiang X W and Fishman R S 1997 *J. Phys.: Condens. Matter* **9** 3417
[17] Lomer W M 1962 *Proc. Phys. Soc.* **80** 489
[18] Laurent D G, Callaway J, Fry J L and Brener N E 1981 *Phys. Rev.* B **23** 4977
[19] Kübler J 1980 *J. Magn. Magn. Mater.* **20** 277
[20] Hirai K 1997 *J. Phys. Soc. Japan* **66** 560
Hirai K 1998 *J. Phys. Soc Japan* **67** 1776
[21] Shi Z P and Fishman R S 1997 *Phys. Rev. Lett.* **78** 1351
[22] Allan G 1979 *Phys. Rev.* B **19** 4774
[23] Grempel D R 1981 *Phys. Rev.* B **24** 3928
[24] Victora R H and Falicov L M 1995 *Phys. Rev.* B **31** 7335
[25] Fu C L and Freeman A J 1986 *Phys. Rev.* B **33** 1755
[26] Blügel S, Pescia D and Dederichs P H 1989 *Phys. Rev.* B **39** 1392
[27] Blügel S, Weinert M and Dederichs P H 1988 *Phys. Rev. Lett.* **60** 1077
[28] Blügel S 1992 *Phys. Rev. Lett.* **68** 851
[29] Fu C L and Freeman A J 1986 *Phys. Rev.* B **33** 1611
[30] Fu C L, Freeman A J and Oguchi T 1985 *Phys. Rev. Lett.* **54** 2700
[31] Vega A, Demangeat C, Dreyssé H and Chouairi A 1995 *Phys. Rev.* B **51** 11 546
[32] Stoeffler D and Gautier F 1995 *J. Magn. Magn. Mater.* **147** 260
[33] Pizzagalli L, Stoeffler D and Gautier F 1996 *Phys. Rev.* B **54** 12 216
[34] Shi Z P, Levy P M and Fry J L 1992 *Phys. Rev. Lett.* **69** 3678
[35] Unguris J, Celotta R J and Pierce D T 1992 *Phys. Rev. Lett.* **69** 1125
[36] Shi Z P and Fishman R S 1997 *Phys. Rev. Lett.* **78** 1351
[37] Fishman R S and Shi Z P 1998 *J. Phys.: Condens. Matter* **10** L277
[38] Fishman R S 1998 *Phys. Rev. Lett.* **81** 4979
[39] Fishman R S 1998 *Phys. Rev.* B **57** 10 284
[40] Fishman R S and Shi Z P 1999 *Phys. Rev.* B **59** 13 849
[41] Hirai K 1999 *Phys. Rev.* B **59** R6612
[42] Niklasson A M N, Johansson B and Nordstöm L 1999 *Phys. Rev. Lett.* **82** 4544
Niklasson A M N 1998 *PhD Thesis* Uppsala Universiteit
[43] Barber M N 1983 *Phase Transitions and Critical Phenomena* vol 8, ed C Domb and J L Lebowitz (London: Academic Press) p 145
[44] Elmers H J 1995 *Int. J. Mod. Phys.* B **9** 3115
[45] Stoeffler D and Gautier F 1993 *J. Magn. Magn. Mater.* **121** 259
[46] Vega A, Stoeffler D, Dreyssé H and Demangeat C 1995 *Europhys. Lett.* **31** 561
[47] Berger A and Fullerton E E 1997 *J. Magn. Magn. Mater.* **165** 471
[48] Bödeker P, Hucht A, Borchers J, Güthoff F, Schreyer A and Zabel H 1998 *Phys. Rev. Lett.* **81** 914
[49] Hucht A 1998, private communication
[50] Slonczewski J C 1995 *J. Magn. Magn. Mater.* **150** 13
[51] Slonczewski J C 1991 *Phys. Rev. Lett.* **67** 3172
[52] Freyss M, Stoeffler D and Dreyssé H 1996 *Phys. Rev.* B **54** R12 677
[53] Kazansky A K and Uzdin V M 1995 *Phys. Rev.* B **52** 9477
[54] Freyss M, Stoeffler D and Dreyssé H 1997 *Phys. Rev.* B **56** 6047
[55] Lovesey S W 1984 *Theory of Neutron Scattering from Condensed Matter* (Oxford: Clarendon)
[56] Bödeker P, Schreyer A and Zabel H 1999 *Phys. Rev.* B **59** 9408
[57] Mori M and Tsunoda Y 1993 *J. Phys.: Condens. Matter* **5** L77
[58] Tsunoda Y, Mori M, Kunitomi N, Yeraoka Y and Kanamori J 1974 *Solid State Commun.* **14** 287
[59] Sonntag P, Bödeker P, Thurston T and Zabel H 1995 *Phys. Rev.* B **52** 7363
[60] Meersschaut J, Dekoster J, Schad R, Beliën P and Rots M 1995 *Phys. Rev. Lett.* **75** 1638
[61] Meersschaut J, Dekoster J, Beliën P, Schad R, Bruynseraede Y and Rots M 1995 *J. Magn. Magn. Mater.* **148** 23
[62] Demuynck S, Meersschaut J, Dekoster J, Swinnen B, Moons R, Vantomme A, Cottenier S and Rots M 1998 *Phys. Rev. Lett.* **81** 2562
[63] Meersschaut J, Dekoster J, Demuynck S, Cottenier S, Swinnen B and Rots M 1998 *Phys. Rev.* B **57** R5575
[64] Keune W, Schatz A, Ellerbrock R D, Fuest A, Wilmers K and Brand R A 1996 *J. Appl. Phys.* **79** 4265
[65] Mibu K, Tanaka S and Shinjo T 1998 *J. Phys. Soc. Japan* **67** 2633
[66] Mibu K, Tanaka S, Kobayashi T, Nakanishi A and Shinjo T 1999 *J. Magn. Magn. Mater.* **198–199** 689
[67] Bauer E 1999 *J. Phys.: Condens. Matter* **11** 9365–85

[68] Hanf M C, Pirri C, Peruchetti J C, Bolmont D and Gewinner G 1989 *Phys. Rev.* B **39** 1546
[69] Krembel C, Hanf M C, Wetzel P, Pirri C, Peruchetti J C, Bolmont D and Gewinner G 1990 *Vacuum* **41** 460
[70] Sonntag P, Donner W, Metoki N and Zabel H 1994 *Phys. Rev.* B **49** 2869
[71] Berlowitz P J and Shinn N D 1989 *Surf. Sci.* **209** 345
[72] Shinn N D and Berlowitz P J 1988 *J. Vac. Sci. Technol.* A **6** 597
[73] Mattson J, Brodsky M B, Ketterson J and You H 1990 *Mater. Res. Soc. Symp. Proc.* vol 160 (Pittsburgh, PA: Materials Research Society) p 231
[74] Kim S K, Jona F and Marcus P M 1996 *Surf. Sci.* **349** 160
[75] Ohresser P, Scheurer F, Carrière B, Deville J P and Dobroiu A 1996 *Surf. Sci.* **352–354** 567
[76] Scheurer F, Ohresser P, Bulou H, Deville J P, Carrière B and Dobroiu A 1997 *Phys. Rev.* B **56** 13 490
[77] Metoki N, Donner W and Zabel H 1994 *Phys. Rev.* B **49** 17 351
[78] Davies A, Stroscio J A, Pierce D T and Celotta R J 1996 *Phys. Rev. Lett.* **76** 4175
[79] Venus D and Heinrich B 1996 *Phys. Rev.* B **53** R1733
[80] Pierce D T, Stroscio J A, Unguris J and Celotta R J 1994 *Phys. Rev.* B **49** 14 564
[81] Lawler J F, van der Kraan R G P, van Kempen H and Quinn A J 1996 *Phys. Rev.* B **53** 11 159
[82] Rouyer D, Krembel C, Hanf M C, Bolmont D and Gewinner G 1994 *Surf. Sci.* **307–309** 477
[83] Rouyer D, Krembel C, Hanf M C, Peruchetti J C, Bolmont D and Gewinner G 1995 *Surf. Sci.* **322** 34
[84] Jandeleit J, Gauthier Y and Wuttig M 1994 *Surf. Sci.* **319** 287
[85] Jungblut R, Roth C, Hillebrecht F U and Kisker E 1991 *J. Appl. Phys.* **70** 5923
[86] Hillebrecht F U, Roth Ch, Jungblut R, Kisker E and Bringer A 1992 *Europhys. Lett.* **19** 711
[87] Walker T G, Pang A W, Hopster H and Alvarado S F 1992 *Phys. Rev. Lett.* **69** 1121
[88] Idzerda Y U, Tjeng L H, Lin H J, Meigs G, Chen C T and Gutierrez J 1993 *J. Appl. Phys.* **73** 6204
[89] Idzerda Y U, Tjeng L H, Lin H J, Gutierrez C J, Meigs G and Chen C T 1993 *Phys. Rev.* B **48** 4144
[90] Fuchs P, Petrov V N, Totland K and Landolt M 1996 *Phys. Rev.* B **54** 9304
[91] Xu Z, Liu Y, Johnson P D and Itchkawitz B S 1995 *Phys. Rev.* B **52** 15 393
[92] Turtur C and Bayreuther G 1994 *Phys. Rev. Lett.* **72** 1557
[93] Klebanoff L E, Robey S W, Liu G and Shirley D A 1984 *Phys. Rev.* B **30** 1048
[94] Klebanoff L E and Shirley D A 1986 *Phys. Rev.* B **33** 5301
[95] Klebanoff L E, Victora R H, Falicov L M and Shirley D A 1985 *Phys. Rev.* B **32** 1997
[96] Berger A and Hopster H 1994 *Phys. Rev. Lett.* **73** 193
[97] Escorcia-Aparicio E J, Choi H J, Ling W L, Kawakami R K and Qiu Z Q 1998 *Phys. Rev. Lett.* **81** 2144
[98] Wiesendanger R, Güntherodt H J, Güntherodt G, Gambino R J and Ruf R 1990 *Phys. Rev. Lett.* **65** 247
[99] Sonntag P, Bödeker P, Schreyer A, Zabel H, Hamacher K and Kaiser H 1998 *J. Magn. Magn. Mater.* **183** 5
[100] Unguris J, Celotta R J and Pierce D T 1992 *Phys. Rev. Lett.* **69** 1125
[101] Unguris J, Cellotta R J and Pierce D T 1991 *Phys. Rev. Lett.* **67** 140
[102] Fullerton E E, Bader S D and Robertson J L 1996 *Phys. Rev. Lett.* **77** 1382
[103] Fullerton E E, Riggs K T, Sowers C H, Bader S D and Berger A 1995 *Phys. Rev. Lett.* **75** 330
[104] Schreyer A, Majkrzak C F, Zeidler Th, Schmitte T, Bödeker P, Theis-Bröhl K, Abromeit A, Dura J and Watanabe T 1997 *Phys. Rev. Lett.* **79** 4914
[105] Ankner J F, Kaiser H, Schreyer A, Zeidler T, Zabel H, Schäfer M and Grünberg P 1995 *J. Appl. Phys.* **81** 3765
[106] Fullerton E E, Adenwalla Felcher G P, Riggs K T, Sowers C H, Bader S D and Robertson J L 1996 *Physica* B **221** 370
[107] Adenwalla S, Felcher G P, Fullerton E E and Bader S D 1996 *Phys. Rev.* B **53** 2474
[108] Schreyer A, Ankner J F, Zeidler Th, Zabel H, Schäfer M, Wolf J A, Grünberg P and Majkrzak C F 1995 *Phys. Rev.* B **52** 16 066
[109] Schreyer A, Ankner J F, Zeidler Th, Schäfer M, Zabel H, Majkrzak C F and Grünberg P 1995 *Europhys. Lett.* **32** 595
[110] Stoeffler D and Gautier F 1991 *Phys. Rev.* B **44** 10 389
[111] Schmitte T, Schreyer A, Leiner V, Siebrecht R, Theis-Bröhl K and Zabel H 1999 *Europhys. Lett.* at press
[112] Pflaum J, Pelzl J, Frait Z, Sturc P, Marysko M, Bödeker P, Theis-Bröhl K and Zabel H 1999 *J. Magn. Magn. Mater.* **198–199** 453
[113] Stierle A, Schreyer A, Hellwig O and Zabel H to be published